Research on Fiber Optic Surface Plasmon Resonance Biosensors: A Review

Qi WANG[1,2,3,4*], Dianyun ZHANG[2], Yizhuo QIAN[2], Xiangyu YIN[2], Lei WANG[2], Shushuai ZHANG[2], and Yuyang WANG[2]

[1]*State Key Laboratory of Synthetical Automation for Process Industries, Northeastern University, Shenyang 110819, China*

[2]*College of Information Science and Engineering, Northeastern University, Shenyang 110819, China*

[3]*Hebei Key Laboratory of Micro-Nano Precision Optical Sensing and Measurement Technology, Qinhuangdao 066004, China*

[4]*State Key Laboratory of Chemo/Biosensing and Chemometrics, Hunan University, Changsha 410082, China*

[*]Corresponding author: Qi WANG E-mail: wangqi@ise.neu.edu.cn

Abstract: Due to the benefits of the high sensitivity, real-time response, no labeling requirement, and good selectivity, fiber optic sensors based on surface plasmon resonance (SPR) have gained popularity in biochemical sensing in recent years. The current research on such sensors is hot in enhancing sensitivity, improving detection accuracy, and achieving the detection of biochemical molecules. The goal of this work is to present a thorough overview of recent developments in the optical fiber SPR biosensor research. Firstly, it explores the basic principles and sensing structures of optical fiber SPR biosensors, focusing on four aspects. Subsequently, this paper introduces three fiber optic surface plasmon biosensors: SPR, localized surface plasmon resonance (LSPR), and long-range surface plasmon resonance (LRSPR). Each concept is explained from the perspective of the basic principles of fiber optic SPR biosensors. Furthermore, a classification of fiber optic SPR biosensors in health monitoring, food safety, environmental monitoring, marine detection, and other applications is introduced and analyzed. Eventually, this paper summarizes the current research directions of SPR biosensors. Meanwhile, it provides a prospective outlook on how fiber optic SPR sensors will develop in the future.

Keywords: Surface plasmon resonance; biosensors; optical fiber sensors; sensitivity

Citation: Qi WANG, Dianyun ZHANG, Yizhuo QIAN, Xiangyu YIN, Lei WANG, Shushuai ZHANG, *et al.*, "Research on Fiber Optic Surface Plasmon Resonance Biosensors: A Review," *Photonic Sensors*, 2024, 14(2): 240201.

1. Introduction

Exceptionally high sensitivity and accuracy, immunity to electromagnetic interference, excellent insulating strength, resistance to corrosion, and interoperability with digital communication systems are the many benefits. Optic fiber sensors [1] have progressed quickly in the last few decades and have been extensively utilized [2]. Surface plasmon resonance (SPR)-based [3] fiber optic sensors have become the most widely used today owing to their benefits of the real-time detection, rapid response, high sensitivity, no contamination, no labeling, low sample usage, and the capacity to detect in real time in the realms of food quality and safety, medical diagnosis [4], and bioengineering [5, 6].

Received: 17 August 2023 / Revised version: 22 October 2023

DOI: 10.1007/s13320-024-0703-7
Article type: Review

The SPR was employed for biosensing and gas detection in 1983 [7]. Biosensors include aspects from several academic fields, such as biology [8, 9], chemistry, physics, medicine [10, 11], and electronics. The biosensor has experienced the vigorous and rapid growth in recent decades due to its many benefits. These advantages include the good selectivity, superior sensitivity, quick analysis, low cost, and the ability to provide online continuous monitoring in complex systems. In addition, its high degree of automation, downsizing, and integration has contributed to its widespread adoption and further development of the field. The principle of fiber optic SPR sensing serves as the foundation for fiber optic SPR biosensors [12, 13]. The refractive index (RI) shift within the evanescent field region of the optical fiber surface is detected by these sensors, which assess the properties of the biomolecule being examined. In fact, while the biomolecular recognition process occurs in the evaporation field region, the metal film's surface changes in the RI. These modifications then appear as adjustments to characteristics like wavelength, angle, and intensity [14]. Using the light's transmitted or reflected intensity as a gauge, among other things, on the fiber optic SPR chip, the biomolecule concentration and presence can be determined. As well as being extensively utilized in environmental monitoring and food engineering, numerous biomolecules, such as proteins, nucleic acids, and viruses, have been detected and examined using fiber optic SPR sensors [15–18].

In this work, a more thorough explanation of the fiber optic SPR biosensing method is provided. Following the introductory section of this paper, we first concentrate on a succinct summary of the fundamental concepts behind surface plasmon exciton resonance as well as the numerous sensor devices used in this context. Next, we review the recently developed SPR, localized surface plasmon resonance (LSPR), and long-range surface plasmon resonance (LRSPR) based sensors. Their applications in biomedicine, environmental monitoring, food engineering, and marine monitoring are also briefly described. Finally, the full text is summarized and directions for further research are proposed.

2. SPR

2.1 Principle

Generally speaking, when a light wave is incident into a light dense medium from a light sparse medium at an angle greater than the critical angle, the phenomenon known as total reflection takes place. In this scenario, even if the light wave cannot penetrate the critical interface between the two mediums, it generates an evanescent wave along a direction parallel to the critical interface. As the distance from the critical surface increases, an exponential decline may be seen in the complex amplitudes of the electric and magnetic fields within the wave that is evanescent [19]. Figure 1(a) illustrates that the presence of free electron gas in the metal allows it to behave like a plasma. When the incident light interacts with the metal, it induces longitudinal oscillations in the electron gas. As a result of the oscillations, the formation of a charge density wave results in the generation of a surface plasma wave that travels along the metal-dielectric contact [20]. The intensity of the monitored reflected light is significantly reduced as a result of the resonance between the metal's surface plasma wave and the evanescent wave [21, 22]. The SPR is the name given to this phenomenon. The profile of the reflected light intensity will exhibit a trough when the corresponding wavelength (or angle) matches the resonance wavelength (or resonance angle) [23]. The division between the wavelength and angle is mainly based on whether the detection system uses wavelength interrogation or angle interrogation. The sensor is sensitive to the RI of the medium attached to the surface of the metal film, and the resonance angle will be different when the properties of the surface medium change or when the amount of attachment changes.

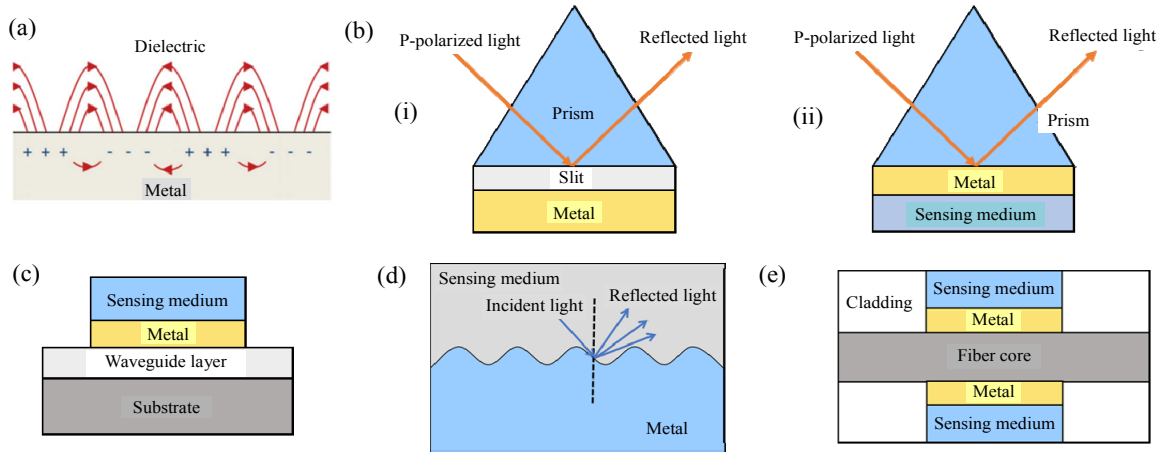

Fig. 1 Schematic structures of the SPR: (a) SPR on a planar metal film; (b) prism-coupled excitation SPR: (i) Otto configuration and (ii) Kretschmann configuration; (c) waveguide coupling device; (d) grating-coupled SPR excitation structure; (e) optic fiber type SPR sensor.

The incident light can be decomposed into S-polarized (TE wave) and P-polarized (TM wave), and these two types of polarized light are perpendicular to each other. Surface plasmon waves are not excited by the electrical field of S-polarized light because it is transverse to the interface and has no impact on the migration of free electrons within the metal; the electric field of the P-polarized light is perpendicular to the interface, which can induce surface charges and form SPR phenomena, which are confined to the surface. Therefore, the necessary condition for generating SPR is the presence of P-polarized light at the incident light [24]. The surface plasma dispersion equation is

$$k_{sp} = k_0 \sqrt{\frac{\varepsilon_1 \varepsilon_2}{\varepsilon_1 + \varepsilon_2}} \tag{1}$$

where k_{sp} is the surface plasma wavevector, k_0 is the wavevector of the light in vacuum, ε_1 is the effective permittivity of the metal, and ε_2 is the permittivity of the surrounding medium. It should be mentioned, however, that the above equations are derived for a simplified case, that is, the case of linear dispersion, and no dissipation of the surface plasma is considered. In practical situations, more complex dispersion models can be considered to describe the behavior of the surface plasma, such as nonlinear dispersion, dissipation, and multilayer structures.

The propagation characteristics of the surface plasmon polariton (SPP) are propagation along the metal/dielectric interface, with the exponential decay along the direction perpendicular to the interface, and the depth of penetration is defined as the depth of penetration of the SPP in the dielectric when the intensity is decayed to the original l/e. The depth of penetration into the medium δ_d and the depth of penetration into the metal δ_m can be obtained:

$$\delta_d = \frac{1}{k_0} \left| \frac{\varepsilon_d + \varepsilon'_m}{\varepsilon_d^2} \right|^{\frac{1}{2}} \tag{2}$$

$$\delta_m = \frac{1}{k_0} \left| \frac{\varepsilon_d + \varepsilon'_m}{(\varepsilon'_m)^2} \right|^{\frac{1}{2}} \tag{3}$$

where δ_d is the penetration depth of the SPP in the medium, δ_m is the penetration depth of the SPP in the metal, k_0 is the wavevector of light in vacuum, ε_d is the dielectric constant of the dielectric, and ε'_m is the real part of the dielectric constant of the metal.

Currently, SPR sensors [25] are divided into four main categories, which will be described separately below.

2.2 Prism coupling

It is based on phase matching when the surface plasmonic excitation wave matches the light wave incident into a medium with a high RI, and it is based on the SPR excitation via the prism coupling principle [26]. The wave vector matching relationship is as follows:

$$k_d = \frac{\omega}{c}\sqrt{\varepsilon_p}\sin\theta = k_{\text{sp}} \tag{4}$$

where ω denotes the angular frequency, c denotes the speed of light in a vacuum, at which light moves in a vacuum, ε_p denotes the prism's dielectric value, k_{sp} represents the surface plasma's transmission constant, θ represents the angle of incidence, and k_d represents the evanescent wave's transmission constant.

The two most commonly used structures to excite the SPR phenomenon are the Otto structure and the Kretschmann structure [27], and the schematic is given in Fig. 1(b). A little space separates the prism from the metal in the Otto construction, the material to be measured exists in this gap, the light is fully emitted through the prism, and some photons pass through to the metal's surface where they interact with the gap to trigger the SPR. One drawback of the Otto structure is the challenge of accurately measuring and reaching the correct dimension of the gap that exists within the prism and the metal, so in practice, the application of the Otto structure of the SPR sensor is relatively limited. In the Kretschmann structure, a metal film is directly coated on the surface of the prism, and the other side of the metal is in contact with the material to be measured. SPR is generated when the evanescent wave has the same wavevector as the plasmon wave on the metal surface, which makes the coupling mechanism more favorable for research and easier to fabricate compared with the Otto structure [28]. Changes in the RI of the external medium to be measured are analyzed by examining the relationship between changes in resonance wavelengths studied by the transmission spectrum. Due to the fast wave's constrained transmission depth, there are some restrictions on the layer thickness of the metallic film, which has an impact on the sensor's sensitivity [29].

2.3 Waveguide coupling

Figure 1(c) illustrates the waveguide coupling apparatus, which is similar in operation to the Kretschmann structure [30]. Based on the optical waveguide processing technology, a metal film is applied behind the waveguide structure, which is placed on a glass substrate. When the light travels through the waveguide-coupled apparatus, some of the transmitted light is present as the evanescent waves, and additionally, the SPR phenomenon is generated when the plasma wave on the metal surface matches the phase of the optical waveguide mode, and the resonance spectra are detected at the waveguides output while the evanescent wave flowing through the metal layer is influenced by the analyte [31]. The coupled optical path of the waveguide is controllable and more miniaturized in size compared to the prism structure.

2.4 Grating coupling

The wave vector matching (5) is satisfied by the grating-coupled SPR [32] excitation structure depicted in Fig. 1(d), which makes use of the metal grating's diffraction effect to adjust the incident light wave vector [33]. By monitoring of the reflected light from the grating, when a minimum value of the reflected light is monitored, the diffracted light wave mode field in the junction plane generated by the representative grating matches the mode field component wave vector of the surface plasma wave, and the two resonate to stimulate the SPR phenomenon, which results in a significant reduction in the diffracted light intensity at that level, so this SPR excitation structure can obtain the SPR spectral peak orientation by examining the variation of the diffracted light intensity:

$$k_d = \frac{2\pi}{\lambda} n_d \sin\theta + m\frac{2\pi}{\Lambda} \quad (5)$$

where k_d is the diffraction light propagation constant, θ is the resonance angle, λ is the incident light wavelength, $m = 0, \pm 1, \pm 2, \cdots$ represents the derivative order, Λ represents the grating's period, and n_d represents the medium's RI.

2.5 Optical fiber coupling

Fiber optic coupled SPR sensors were proposed by R. C. Jorgenson *et al*. in 1993 [34]. Fiber optic SPR sensors, contrary to the traditional prism-coupled SPR sensors, can be fitted to a variety of complicated situations because of their thin and flexible nature, resistance to electromagnetic interference, and resistance to high temperature corrosion. Moreover, due to the small size of fiber optic SPR sensors, they can penetrate into slits that are difficult to access by prism-coupled sensors and can be detected over long distances. In addition, fiber-coupled SPR sensors can be made into various probe sensors owing to their unique structural features. Due to these advantages, the fiber-coupled SPR sensors [35] have a great prospect for gas and environmental detection.

The optical fiber SPR sensor is realized by using the coupling of the evanescent wave and surface plasma wave (SPW) excitation SPR phenomenon. In the optical fiber propagation of the incident light from the core (light dense medium) to the metal film (light sparse medium) in the core and the metal film interface to generate the evanescent wave, the evanescent wave perturbation of free electrons on the surface of the metal makes it continue to oscillate at the interface to form a surface plasma wave, when the frequency of the incident light and the vibration frequency of the SPW are the same. The majority of the energy of the incident light will be absorbed by the SPW in order to maintain its vibration, and accordingly, the spectral map of the incident light will appear in an absorption peak. Changes in the RI of the external environment can change the resonance conditions of the SPR, resulting in a shift of the resonance wavelength in the long-wave direction (redshift) or in the short-wave direction (blueshift).

Optic fiber-coupled biosensors [36] make use of the evanescent wave generated on the core surface when the incident light travels through the fiber as an excitation source to find the target object on the core surface. Figure 1(e) displays the schematic representation of the SPR sensor construction. The standard procedure is to coat a metal or responsive film outside of the cladding by partially removing the fiber's coating layer, or removing the cladding layer as well and coat the metal or sensitive film directly outside the fiber core, then using this area as the sensing area to contact the sample to be measured for detection.

3. Surface plasmon-based sensors

The advantage of optical fiber-coupled SPR sensors [37] over other SPR sensors is that they are simple to use, take up relatively little space, are highly sensitive, and exceptionally stable. Therefore, in recent years, more and more researchers have devoted themselves to this study [38] in order to improve their performance.

3.1 SPR sensors

3.1.1 Structurally improved fiber optic SPR sensor sensitivity

So far, there have been various types of optic fiber structures, mainly D-type probes, U-type probes, and tapered probes. The main types of optical fibers are singlemode fibers (SMFs), multimode fibers (MMFs), photonic crystal fibers (PCFs), plastic optical fibers (POFs), and fiber Bragg gratings (FBGs). A brief summary of the research on each of these structures is presented below.

A. D-shaped probes

The D-type fiber has a side-polished fiber

cladding, which improves the susceptibility of the cladding modes, its mechanical properties, and the high sensitivity. In recent years, D-type based fiber optic sensors have been widely used for the detection of various environmental parameters, such as the RI, strain temperature, and magnetic field.

A symmetric SPR sensor with a double-D form made of photonic crystals with the directional power interaction between two fibers was proposed by C. Liu [39] in 2018 to enhance the sensor performance. Figure 2(a)(i) depicts the sensor's two symmetric double-D-shaped photonic crystal fibers, and Fig. 2(a)(ii) depicts the fundamental mode electric field intensity distribution, the fiber's core and cladding are represented by Regions A and B, which stand separately. In comparison to a single D-shape sensor, a double D-shape sensor has a much better amplitude sensitivity with the exception of 1.40 and 1.41, as shown in Fig. 2(b), which contrasts the sensitivity to amplitude and wavelength around the two types of sensors. In the same year, X. Chen [40] proposed a novel D-type photonic crystal fiber RI sensor based on the SPR that stimulates the plasma mode in an open-loop channel covered with a gold film. Figure 2(c) depicts the schematic diagram of the suggested D-type PCF. The structure is made up of two hexagonal rings, and additionally, as the analyte RI (n_a) is changed from 1.20 to 1.29, as seen in Fig. 2(d), the wavelength of the resonance shifts. The fitting results are displayed in the inset table. The slope denotes the sensitivity of the suggested SPR-PCF sensor, which, at n_a=1.29, has a maximum spectral sensitivity of 11 055 nm/RIU and a maximum resolution of 9.05×10^{-6} RIU.

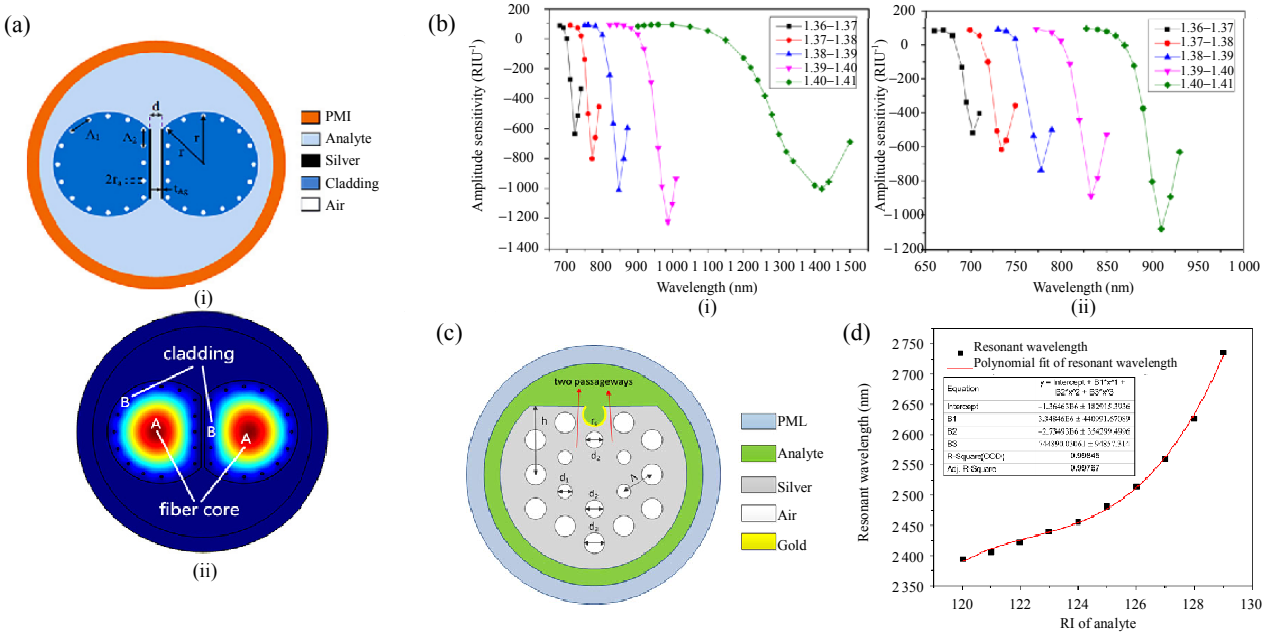

Fig. 2 D-shaped probes schematic (a): (i) symmetric double D-shaped PCFs-SPR sensor cross-section and (ii) basic modal electric field intensity distribution (Fig. 1 in [39]), (b) changes in the analyte RI of 0.01 and the relationship between amplitude sensitivity and wavelength for (i) double D-shaped sensor and (ii) single D-shaped sensor (Fig. 11 in [39]), (c) schematic of the D-shaped PCF sensor that is being proposed (Fig. 1 in [40]), and (d) variation of the resonance wavelength across the insertion table and the shift of the analyte RI from 1.20 to 1.29 is due to a polynomial fit (Fig. 9 in [40]).

The MXene ($Ti_3C_2T_x$) covered the high sensitivity D-type PCF for the SPR biosensor was proposed by F. Mumtaz *et al.* [41] in 2022. The sensor's schematic cross-section can be seen in Fig. 3(a)(i), and Fig. 3(a)(ii) shows the stacked and drawn schematics of its geometry. With an analyte's RI of 1.42, the recommended sensor has a maximum RI sensitivity of 47 260 nm/RIU, which is 1.7 times

greater than the sensitivity achieved by a single Au film SPR sensor. The setup for the experiment is displayed in Fig. 3(b). In addition, to detect a wider range of biological analytes, it makes use of a third-order polynomial fit function, which correlates to the wavelength shift (i.e., RI of 1.30 to 1.43). A D-type SMF SPR sensor for detecting DNA hybridization was developed by J. Gao *et al*. [42] in 2023 based on composite nanostructures of single-layer graphene and hyperbolic metamaterial (HMM). Figure 3(c) shows the preparation steps for the designed sensor. The proposed sensor's sensitivity and figure of merit are determined through experiments to be 5 000 nm/RIU and 40 RIU^{-1}, respectively. The sensor is utilized to monitor DNA molecule hybridization based on ideal settings, and the affinity and reaction rate of DNA hybridization are analyzed based on molecular reaction dynamics.

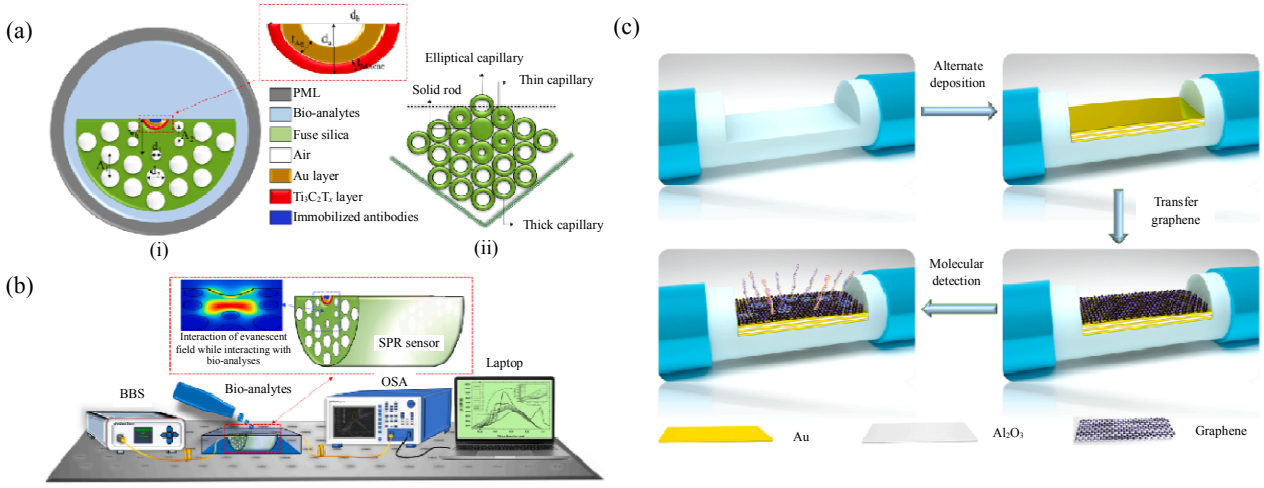

Fig. 3 D-shaped probes schematic (a): (i) cross-sectional diagram and (ii) suggested sensor's stacked and sketched configuration (Fig. 1 in [41]), (b) proposed experimental configuration for evaluating bio-analytes (Fig. 2 in [41]), and (c) process of making the monolayer graphene/HMM/D-SMF SPR sensor (Fig. 3 in [42]).

B. U-shaped probes

Since the U-shaped bent fiber optic sensor [43] was proposed in 1996, it has been widely used in many fields, such as medicine, biotechnology, and food safety. It has been shown that U-bent SPR sensors have the good sensitivity and can convert low-order modes into high-order modes [44]. Compared with other structures, U-bent fibers are simple to fabricate and can be used as point sensors.

A U-shaped bending fiber SPR sensor constructed from graphene/AgNPs was proposed by C. Zhang [44] in 2017. This sensor was made in accordance with the steps in Figs. 4(a) and 4(b), which show the U-shaped SPR sensor setup for determining the resonance wavelength change. According to the findings, the resonance wavelength shifts of 90% ethanol and 20% glucose aqueous solutions are as high as 32 nm and 16 nm, respectively. The suggested sensor is anticipated to offer the new detection possibilities in the areas of medicine, biotechnology, and food safety. A self-compensating, label-free, and interference resistant SPR fiber optic biosensor constructed using the cascaded U-shaped MMF and SMF was proposed by Q. Wang [45] in 2020 to improve the stability and anti-interference property to respond of the sensor in the detection of complex biological fluids. Figure 4(c) displays the fabrication process, and Fig. 4(d) displays the fiber surface modification process, which can detect human immunoglobulin G (IgG) with a sensitivity of 0.192 nm/(g/mL) and a minimum limit of detection (LOD) of 0.104 μg/mL. The multichannel fiber-optic SPR sensor enables both the recognition of specific binds as well as the

detection of a variety of analytes. W. Zhang [46] published the first research on a few-mode fiber (FMF) based and temperature-insensitive salinity sensor in 2023. The results demonstrate that the suggested U-shaped FMF sensor's sensitivity reaches up to 1.847 nm/% in the salinity vary of 0%–10%, as illustrated in the schematic and microscopic schematics of the device in Fig. 4(e). It exhibits a temperature insensitive feature between 5 ℃ and 30 ℃. This sensor has the benefits that it is temperature-insensitive and has a straightforward preparation method, which makes it more suitable for use in measuring the temperature and salinity of saltwater than the typical fiber optic sensors. To improve sensor performance, Z. H. Ren [47] presented a core mismatch U-shaped and tapered arm optical fiber SPR sensor in 2023. It has a high comprehensive evaluation index. Figure 4(a) depicts the fabrication procedure, whereas Fig. 4(b) shows the sensor structure depending on a microscope. The addition of the SMF according to simulation and experimental data, extends the effective sensing region, and deepens the resonant valley (RVD). The results of the studies indicate that there is an ideal value for the gold film thickness and bending amount after the addition of the SMF and tapered structure. The complete evaluation index of the sensor is 2.5 times greater after parameter optimization than that of the U-type multimode fiber sensor.

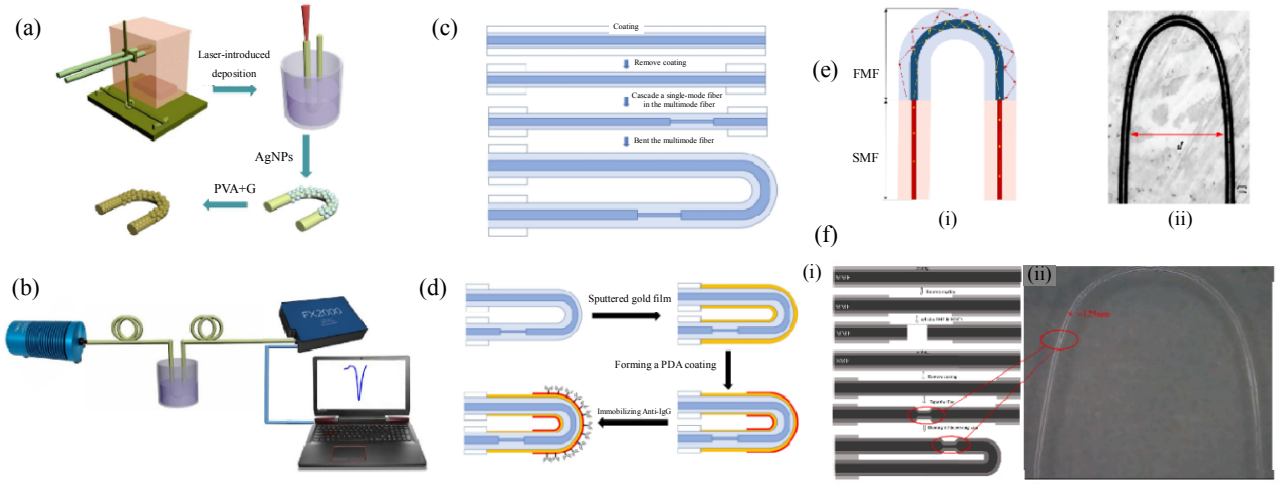

Fig. 4 U-shaped probes schematic: (a) diagrammatic representation of the U-shaped fiber SPR sensor's manufacturing process (Fig. 1 in [44]); (b) diagrammatic representation of the experimental setup (Fig. 2 in [44]); (c) illustration of the sensor structure's manufacturing process (Fig. 4 in [45]); (d) diagram of the process of fiber surface modification (Fig. 5 in [45]); (e): (i) U-type FMF sensor's design and (ii) microscopic viewpoint (Fig. 1 in [46]); (f) fabrication process of the sensing fiber structure (Fig. 3 in [47]).

C. Tapered probes

Small but accurate and sensitive sensors are needed for diverse biomedical, physical, and chemical measurements. In this case, tapered optical fibers have important applications, which are suitable for a variety of sensors, such as humidity, strain, RI, and temperature sensors [48].

Y. Zhao *et al*. [49] suggested a novel RI sensor in 2015, which utilized a multi-tapered SMS (S: singlemode fiber; M: multimode fiber) fiber topology. By sharpening several tapers within the MMF portion that comprises the SMS fiber structure, three, five, and eight tapers are produced for the sensor, which can be inferred that as the number of tapers increases, so does the measurement sensitivity. The results of experiments indicate that the RI sensitivity in the RI range of 1.3333–1.3737 is 261.9 nm/RIU when there are eight tapers. Y. Al-Qazwini *et al*. [50] produced a short tapered MMF-based SPR sensor in the same year. Figure 5(a)(i) shows the tapered fiber under a microscope, which is made up of three contiguous parts: two narrow transition areas and a narrow, uniformly sized, and tapering waist section. Having

a sensitivity range of 1 600 nm/RIU–2 000 nm/RIU, a spectral width of 140 nm–220 nm, and a standard MMF that is 25 m–45 m long with a short tapered length of 3 mm–5 mm in total, Fig. 5(a)(ii) depicts the real sensor image that is created, and Fig. 5(b) depicts the experimental setup utilized to quantify the SPR transmission spectrum. A unique tapered bi-metallic fiber sensor with an SPR foundation was proposed by N. Goswami *et al.* [51] in 2016. It allows for the detection of RI variations by the excitation of radially polarized light. The entire Ag-Au coating tapered MMF with the SPR alongside radially polarized beam and light trace is depicted in Fig. 5(c). Based on the results, it can be seen that the output response sensitivity of the wavelength detection technique is 10 times greater than the corresponding value of the p-polarized light, and the output response sensitivity of the intensity detection technique is 2.307 times much greater than the p-polarized light. RI sensing using a high-sensitivity surface developed around an MMF-tapered hollow core fiber (THCF)-MMF design was proposed by C. Teng *et al.* [52] in 2022. A gold film has been put on one side of the THCF in the MMF-THCF-MMF segment of the THCF, which is connected by two MMFs. The sensitivity of this sensor is greatly enhanced at the big RI, according to experimental findings. The MMF-THCF-MMF probe's sensitivity may be increased to 7 592.25 nm/RIU at the RI of 1.40, using a standard HCF with a core diameter of 30 μm, as well as a taper ratio of 3.3.

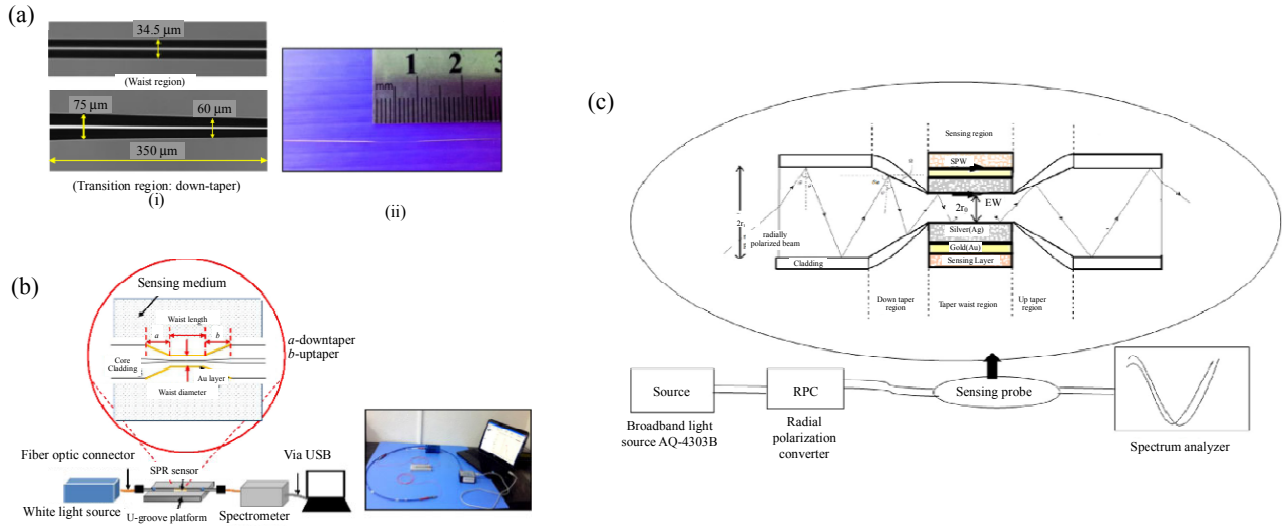

Fig. 5 Tapered probes schematic: (a): (i) picture of the tapered fiber under a microscope and (ii) diagram of the real sensor that is created (Fig. 1 in [50]); (b) diagrammatic representation of the experimental setup (Fig. 2 in [50]); (c) in a schematic illustration, the tapered fiber sensor probe is displayed (Fig. 1 in [51]).

D. Other probes

In addition to the several structures of probes mentioned above, many other structures of probes emerged in later studies that could also enable the sensor performance to be enhanced, and a brief review of the other probes is given below.

A concave-convex photonic crystal fiber (PCF) based on indium tin oxide (ITO) coupled with a square channel was Z. Yang *et al.*'s idea for an SPR sensing technique in 2018 [53]. Based on the finite element method, the characteristics of the modes of light wave propagation in the PCF are examined. As seen in Fig. 6(a), the structure's cross section primarily comprises four hexagonal stomatal rings arranged around the central stomatal opening. The sensor's operating wavelength is between 1 270 nm and 1 692 nm, and its maximum wavelength sensitivity is between 1 700 nm/RIU and 10 700 nm/RIU when the dynamic RI falls within the range of 1.19 to 1.29.

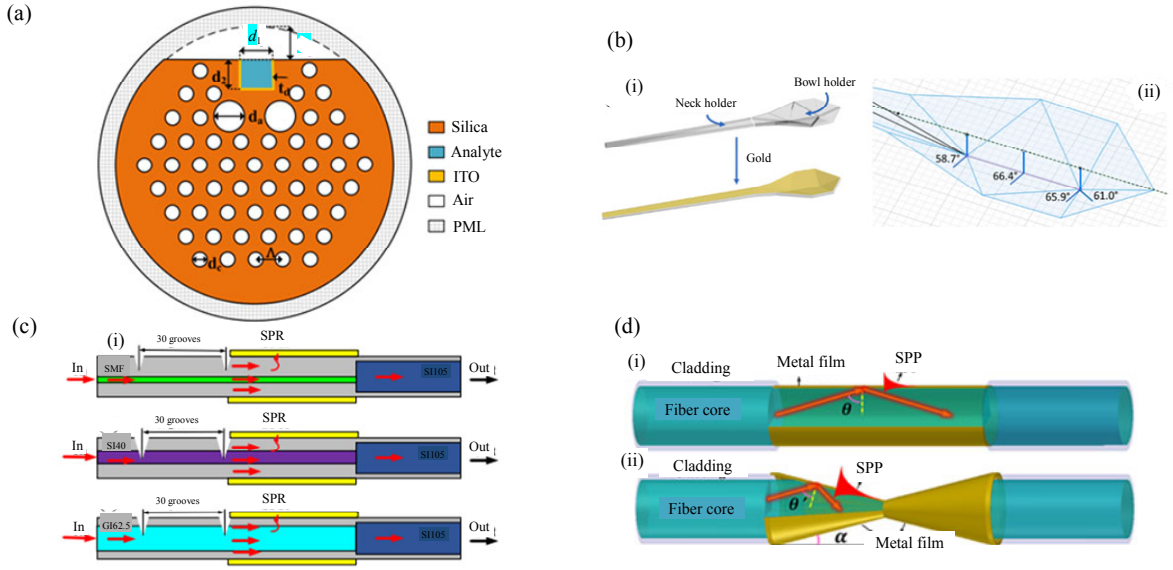

Fig. 6 Other probes schematics: (a) picture of the PCF-SPR sensor in cross-section (Fig. 1 in [53]); (b): (i) optical waveguide's spoon-shaped geometry [to stimulate plasma processes, a thin gold layer (about 60 nm) is applied to the waveguide's upper surface] and (ii) detail of the bowl angle (Fig. 1 in [55]); (c) schematic representation of a fiber clad SPR sensor with the V-groove construction for (i) SMF, (ii) step-RI MMF, and (iii) gradient-RI MMF fiber (Fig. 8 in [56]); (d) diagrams of the proposed biconical fiber SPR sensor and an MMF SPR sensor built on the industry standards are depicted in (i) and (ii), respectively (Fig. 1 in [57]).

Using the wavelength division multiplexing technology, L. Li *et al*. [54] suggested a sawtooth-type dual-channel fiber SPR sensor in 2022. By repeatedly cutting V-shaped grooves into a stepped multimode fiber using a CO_2 laser, the sawtooth structure is created. The first polymeric multimode waveguide with a ground-breaking scoop geometry was put out by N. Cennamo *et al*. [55] for the creation of SPR biological sensors in the same year. This multisensor is based on molecularly imprinted nanoparticles and antibodies, and its structure is schematically depicted in Fig. 6(b), which can detect more than 8 orders of magnitude of the protein concentration. Using a CO_2 laser on the basis of a V-shaped notch construction, L. Li *et al*. [56] demonstrated a fiber-clad SPR sensor. The sensor probe structure is shown in Fig. 6(c): (i) the sensor probe diagram of the SMF V-slot structure, (ii) the sensor probe diagram of the step RI fiber V-slot structure, and (iii) the sensor probe diagram of the gradient RI fiber V-slot structure. According to the experimental findings, the RI sensitivity of the three sensors for the SMF is 2 811.34 nm/RIU for the gradient RI fiber is 1 862.33 nm/RIU, and for the step RI fiber is 1 418.85 nm/RIU, while they have respective sensitivity to curvature values of 0.42 nm/m^{-1}, 1.03 nm/m^{-1}, and –6.59 nm/m^{-1}. S. Zhang *et al*. [57] presented an extremely sensitive, incredibly small, and corrosion-resistant dual-tapered fiber-optic SPR sensor to gauge the salinity of seawater. In Fig. 6(d), the newly developed biconical fiber optic salinity sensing structure is shown beside the traditional MMF SPR sensing structure. According to experimental findings, the biconical fiber optic SPR sensor's sensitivity is generally correlated with a particular range of grinding angles. In the range of 1.3333 to 1.3541, when the grinding angle α reaches 14°, the sensitivity is the highest, 3 965 nm/RIU, and the sensor also has a certain repeatability and stability.

A dual-channel S-based fiber-clad SPR sensor was put forth by Y. Wei *et al*. [58] in 2023. The sensing fibers for Channels I and II are respectively

an FMF and an MMF with a gradient RI. The findings indicate that the resonant working bands for Channels I and II are 627.66 nm–759.78 nm and 518.24 nm–658.20 nm, respectively, with an average sensitivity of 2 540.77 nm/RIU and 2 691.54 nm/RIU, respectively, in the RI detection range covering 1.333–1.385.

3.1.2 Improving fiber optic SPR sensor sensitivity in materials

In order to enhance the performance, the sensor can be made more sensitive by combining other materials with it. The current state of sensitization is discussed below in terms of zero-dimensional materials, one-dimensional (1D) materials, and two-dimensional (2D) materials.

A. Zero-dimensional materials

Materials with zero dimension are those, in which electrons cannot freely move, such as quantum dots and nanoparticles. In 2019, X. Jiang *et al*. [59] prepared the MWCNT/PtNPs fiber optic SPR sensor and conducted the experimental verification of the sensor's performance. Figure 7(a) shows the SPR probe sensing structure of MWCNT/PtNPs.

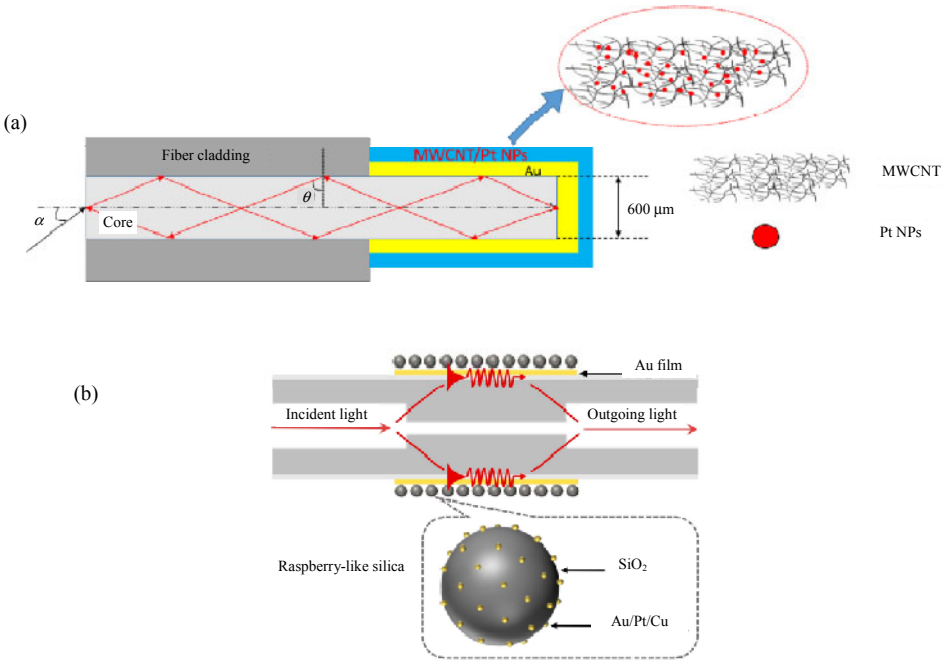

Fig. 7 Zero-dimensional materials part diagram: (a) diagram of the SPR probe sensing structure for MWCNT/PtNPs (Fig. 6 in [59]) and (b) silica-aided SPR sensor with a raspberry-like schematic (Fig. 1 in [61]).

The outcomes demonstrate that carbon nanotubes can increase the fiber optic SPR sensors' sensitivity. MWCNT/PtNPs composites have the potential for further enhancing the sensors' sensitivity and high figure of merit (FOM). In 2020, C. Liu *et al*. [60] proposed a method to model the sensing effect of SMF optic SPR sensors with metal nanoparticles modifying the tapered-angle structure. After parameter tuning, a sensitivity of 5 140 nm/RIU is reached, which opens up a new line of inquiry for researchers enhancing the fiber optic SPR sensors' sensitivity. The angle of light's incidence determines the grinding angle of the sensor probe. A fiber optic SPR sensor with an FOM with raspberry silica assistance was proposed by Q. Wang *et al*. [61] in the same year. By combining several noble metal nanoparticles (AuNPs, PtNPs, and CuNPs), raspberry-like silica particles are created, allowing researchers to assess the effects of different nanoparticles on sensing performance.

Figure 7(b) presents a diagram of the sensor architecture. According to sensing studies, the sensor is most effective with AuNPs raspberry-like silica, which makes it sensitive to 5264.3 nm/RIU.

B. 1D materials

A 1D material is one in which electrons are free to move in only one nanoscale direction (linear motion), such as nanowires, nanorods, and nanotubes. Single-walled carbon nanotubes (SWCNTs) were used as the top layer in A. K. Mishra *et al*.'s 2017 proposal [62] for a fiber-coupled RI sensing probe based on the SPR. Figure 8(a)(i) displays the sensing probe's schematic diagram. In Fig. 8(a)(ii), two types of carbon nanotubes – single-walled and multi-walled (MWCNTs) – are shown schematically. In order to create highly sensitive probes, the thicknesses of the various constituent layers are adjusted. The resultant probes have a sensitivity of 9.78 m/RIU in the electromagnetic spectrum's infrared area. J. Y. Jing *et al*. [63] developed two carbon nanotubes (CNTs) deposited Au film PCF-SPR sensors in 2018 (CNTs/Au-PCF sensor) and one carbon nanotube deposited Ag film PCF-SPR sensor (CNTs/Ag-PCF sensor), and a number of tests were carried out using them to investigate the RI sensing capabilities of the carbon nanotube deposited SPR sensor. The findings suggest that adding a CNT layer could increase the fiber optic SPR sensors' sensitivity, and the effect on Au-PCF sensors is more significant. Additionally, the feasibility of a CNTs/Au-PCF sensor for biomolecule detection is evaluated using the target analyte bovine serum albumin (BSA), demonstrating the promising use of CNTs in biochemistry. Using the hemoglobin oxygen transport mechanism sensor and fiber optic SPR theory, M. Luo *et al*. [64] designed and tested a novel dissolved oxygen sensor in 2021. A gold film is applied on the optical fiber sensing region's surface, which is subsequently modified with carbon nanotubes on one side and hemoglobin on the other. According to the experimental research, the sensitivity of the sensor upgraded with carbon nanotubes is found to be 2.8 times more comparable to the sensor modified only with hemoglobin, with an increased linearity and a lower detection limit of 0.01 mg/L. In 2022, M. F. Naief *et al*. [65] created a brand-new composite nanomaterial called multi-walled carbon nanotubes (MWCNTs) covered with platinum nanoparticles (Pt-NPs), and the composite was used in a new therapeutic human PC3 cell line. The local treatment of prostate cancer may benefit from the combined

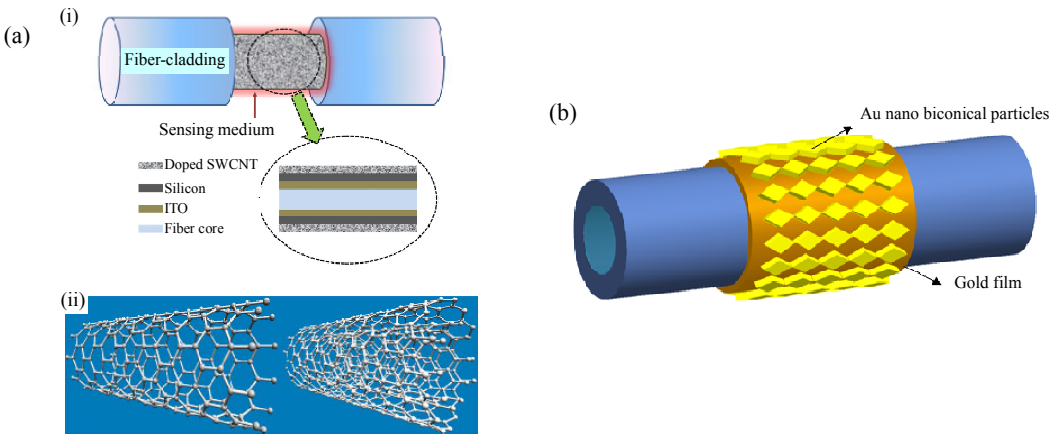

Fig. 8 1D materials part diagram: (a) illustration of the sensing probe using MWCNTs and SWCNTs (Fig. 1 in [62]) and (b) schematic of the gold nanobiconical particle modified sensor's three-dimensional (3D) structure (Fig. 2 in [66]).

use of MWCNTs and Pt-NPs in photothermal therapy in a concentration- and time-dependent way. In the same year, Q. Wang *et al*. [66] proposed a coreless optical fiber-based coupling-improved SPR sensor and its performance was boosted by the addition of gold nanobiconical particles. Figure 8(b) provides a schematic for the proposed sensor. The improved gold nanobiconical particle sensor is 64% more sensitive than the conventional gold film SPR sensor, with a sensitivity of 3 514 nm/RIU, and had a 24% higher quality factor.

C. 2D materials

2D materials, including MXene, graphene, boron nitride (BN), molybdenum disulfide (MoS_2), tungsten disulfide (WS_2), and molybdenum diselenide ($MoSe_2$), are those in which electrons in order are free to travel on the nanoscale (planar motion) in just two dimensions. H. Fu *et al*. [67] suggested an optical fiber SPR biosensor in 2015 that used a gold film coated with a layer of graphene as the sensing layer. A four-layer modality is used to undertake a theoretical analysis of the suggested fiber optic biosensor. The results show that the sensitivity of the proposed SPR fiber optic biosensor could be greatly enhanced by incorporating a graphene sensing layer in the SPR fiber. Q. Wang *et al*. [68] suggested a graphene oxide/silver-plated polymer-clad silica fiber optic SPR biosensor in 2018. It has the good sensitivity and a low detection limit. The produced SPR sensor, which has an RI sensitivity of 3311 nm/RIU, is schematically represented in Fig. 9(b) and the functionalization procedure is shown in Fig. 9(a). The graphene oxide/silver sensing surface is then further functionalized in order to detect SPA and goat anti-human IgG at different concentrations with a high sensitivity of 0.4985 nm/(g/mL) as well as a low LOD of 0.04 g/mL.

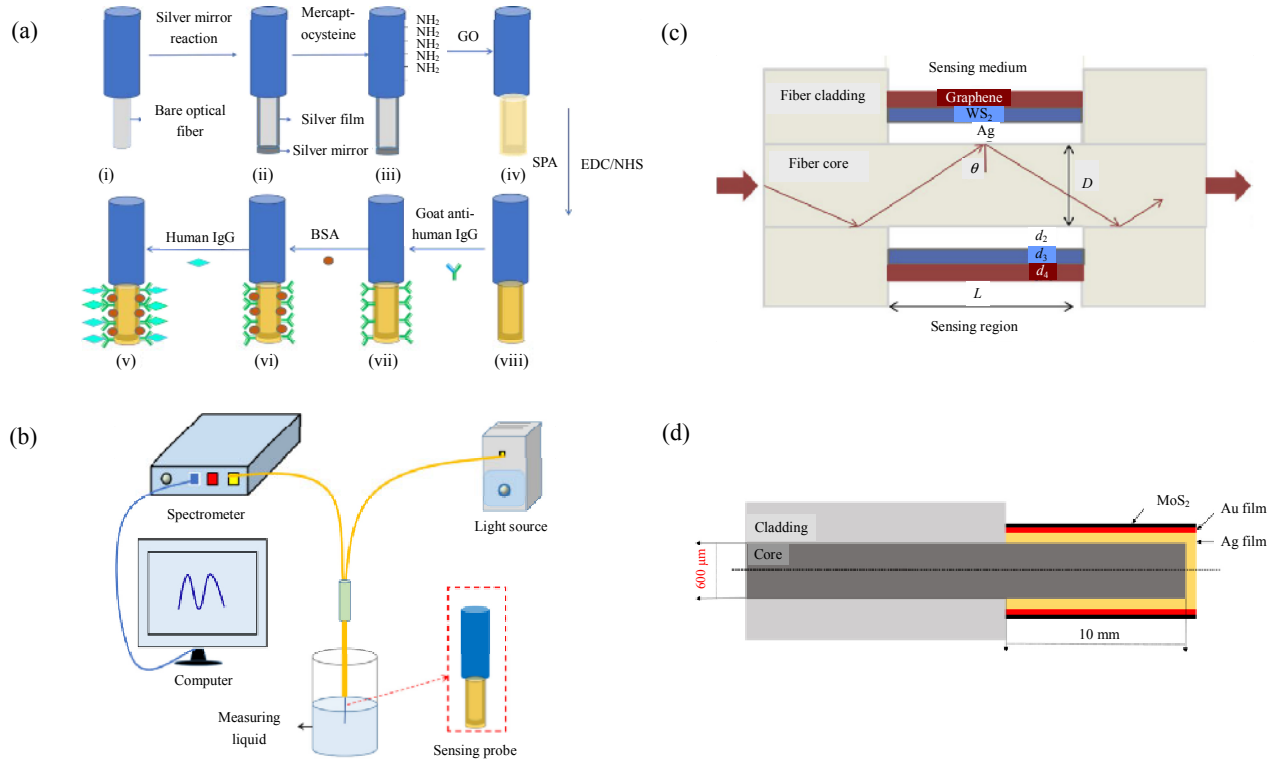

Fig. 9 2D materials part diagram: (a) process for functionalization illustration ([68], Fig. 2), (b) experimental system is depicted in a schematic diagram ([68], Fig. 3), (c) suggested SPR biosensor's structural diagram ([69], Fig. 1), and (d) model of a gold/silver bimetallic fiber SPR sensor covered with MoS_2 ([70], Fig. 2).

A tungsten disulfide graphene-coated fiber optic SPR biosensor was created and quantitatively studied by M. S. Rahman *et al*. [69] in 2019 to increase the sensor's sensitivity and stability. The sensor uses graphene as a cladding layer and introduces tungsten disulfide on graphene, and its structure is shown in Fig. 9(c), which shows that with a layer of WS_2 coated with graphene, the sensor exhibits a 3200 nm/RIU exceptionally high sensitivity. According to Q. Wang *et al*.'s proposal [70] in 2020, Fig. 9(d) shows a schematic representation of a molybdenum disulfide (MoS_2) nanosheet-based bimetallic optical fiber SPR sensor. The outcomes demonstrate that the addition of MoS_2 improves the sensor's sensitivity, which is 3061 nm/RIU with an FOM value of 23.29 RIU^{-1}. Using 2D hydroxide molybdenum-doped (HMO) nanodiscs integrated onto a gold-plated optical fiber, T. Li *et al*. [71] suggested a sensitivity-enhanced SPR sensor in the same year. Within a predetermined thickness, the HMO ion doping concentration, as well as the RI sensitivity, correlated positively, having a maximum sensitivity of 4566 nm/RIU and an average sensitivity improvement of 84.5%.

3.2 LSPR sensors

The charge distribution on the surface of a metal formed as a nanoparticle will be disturbed by external electromagnetic waves, and when the frequency of the electron oscillation and the frequency of the external excitation light coincide, it results in a significant oscillation of the electron cloud. This causes the development of local surface plasmon excitations (LSPs), which culminate in the LSPR.

Using a cone-based construction, H. H. Jeong *et al*. [72] suggested a new fiber optic RI sensor in 2013 and fixed AuNPs on its surface to make the proposed cone structure into a fiber optic LSPR sensor. The fiber optic LSPR sensor with a conical structure can detect the RI by adjusting the peak wavelength and changing the strength of the reflected resonance. In the same year, M. Rani *et al*. [73] suggested and theoretically evaluated a fiber optic sensor based on the LSPR. According to Fig. 10(a), the suggested sensing system is made up of an optical fiber core, a nanoparticle layer, and a sensing medium.

ITO, Au, Ag, and Cu nanoparticles are the four materials taken into consideration in the study, and the sensitivity of each layer of nanoparticles at various thicknesses and particle sizes is numerically examined. It is demonstrated that the LSPR sensor's sensitivity is 6240 nm/RIU for ITO nanospheres with a particle size of 20 nm, which outperforms the nanosphere LSPR sensors of the other three materials. M. H. Tu *et al*. [74] suggested a gold nanostructure-based optical fiber LSPR sensor in 2014 and carried out much measurement of the RI. The results reveal that the recommended sensor's sensitivity is greatly raised up to 1933 nm/RIU and are illustrated in Fig. 10(b), which is a schematic diagram of the LSPR sensor system. The LSPR biochemical fiber sensor's functionality was further improved in 2015 by Y. J. He *et al*. [75], who developed an innovative design model with a short length (74.34779 μm), a high resolution (–110 dB), and a high wavelength sensitivity (93987 nm/RIU). Figure 10(c) shows the side structural diagram of the sensor's LSPR biological fiber optic device. A unique LSPR sensor based on a U-shaped bent plastic optic fiber (U-POF) was proposed by S. Jiang *et al*. [76] in 2017. According to the findings, the range of RIs from 1.3300 to 1.3657 has a sensitivity of 700.3 nm/RIU.

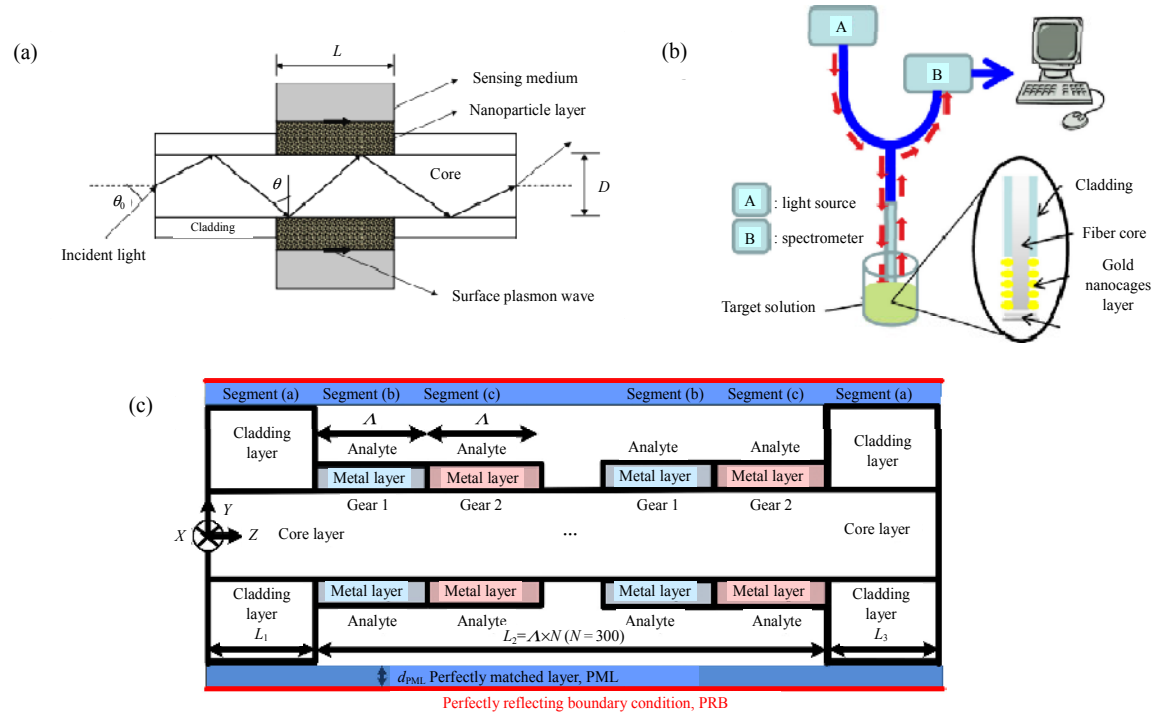

Fig. 10 LSPR part diagram: (a) schematic illustration depicts the LSPR-based fiber optic sensor (Fig. 1 in [73]), (b) LSPR sensor system is depicted in a schematic diagram (Fig. 2 in [74]), and (c) LSPR biochemical fiber sensor's novel side structure (Fig. 1 in [75]).

H. M. Kim *et al*. [77] suggested a localized SPR biosensor using fiber optic surface nanopatterned gold particles in 2018 to increase the robustness and manufacturing repeatability of fiber optic localized SPR (FO LSPR) sensors and performed prostate-specific antigen (PSA) immunoassay that could measure PSA up to 0.1 pg/ml. For the purpose of identifying cancer cells and assessing the N-glycans on their surface, Z. Luo *et al*. [78] developed a cellular sensing method using the U-shaped fiber optic LSPR in 2019. The U-shaped fiber optic LSPR device is depicted in Fig. 11(a). By altering the size of gold nanoparticles and also the concentration of Con A, the U-shaped fiber optic LSPR cell sensor is able to be made extremely sensitive for the detection of cancer cells, with an LOD of up to 30 cells/mL with the excellent linearity in a broad linear range (1×10^2 cells/mL–1×10^6 cells/mL). In 2019, H. Song *et al*. [79] suggested a graphene oxide/triangular nanosilver structure LSPR fiber optic sensor. In Fig. 11(c), the experimental setup for creating a U-shaped fiber optic LSPR sensor using spherical and triangular nanosilver is depicted schematically, and Fig. 11(b) illustrates the nanosilver sensing probe. The triangular nanosilver particle sensor has a sensitivity of 1116.8 nm/RIU compared to the spherical nanosilver particle sensor's 342.7 nm/RIU. The difference between the LSPR and traditional SPR sensing in terms of the sensitivity and sensing capability can be filled by densely organized gold nanoparticles (AuNPs) that are evenly scattered across optical fibers. The optical fiber LSPR sensing device used by M. Lu *et al*.'s [80] biosensor for protein immunoassay and RI sensing is depicted in Fig. 11(d). The outcomes show that the sensor's sensitivity is able to be employed as a biosensor because it has an LOD of 1.1 nM to detect human IgG.

H. M. Kim *et al*. [81] proposed an LSPR sensor with a hybrid construction of a dielectric film and a bilayer of gold nanoparticles on an optical fiber in 2021 to increase the sensitivity of the sensor. Monolayers and bilayers with AuNPs are prepared

on optical fibers, respectively. The results show that the double layer AuNPs improves the sensor sensitivity by roughly 2.3 times over the single layer. To achieve precise monitoring of human glucose levels in 2022, G. Li *et al*. [82] created a new LSPR sensor based on a quadruple conical shape. According to the experimental findings, the linear range of 0 mM–10 mM has the sensitivity and detection limits of 1.04 nm/mM and 0.24 mM, respectively, for the functionalized probe structure.

The detection method known as the LSPR is based on the SPR of metal nanoparticles. The benefits of the LSPR in the biological sector include the changeable wavelength and highly sensitive detection, and the technology is relatively low-cost, which is suitable for low-cost and high-throughput studies. However, the method has great limitations and cannot achieve the simultaneous detection of multiple biological macromolecules. Moreover, because of its high sensitivity, there is a risk of false detection, so relevant research needs to be enhanced to improve its accuracy and precision.

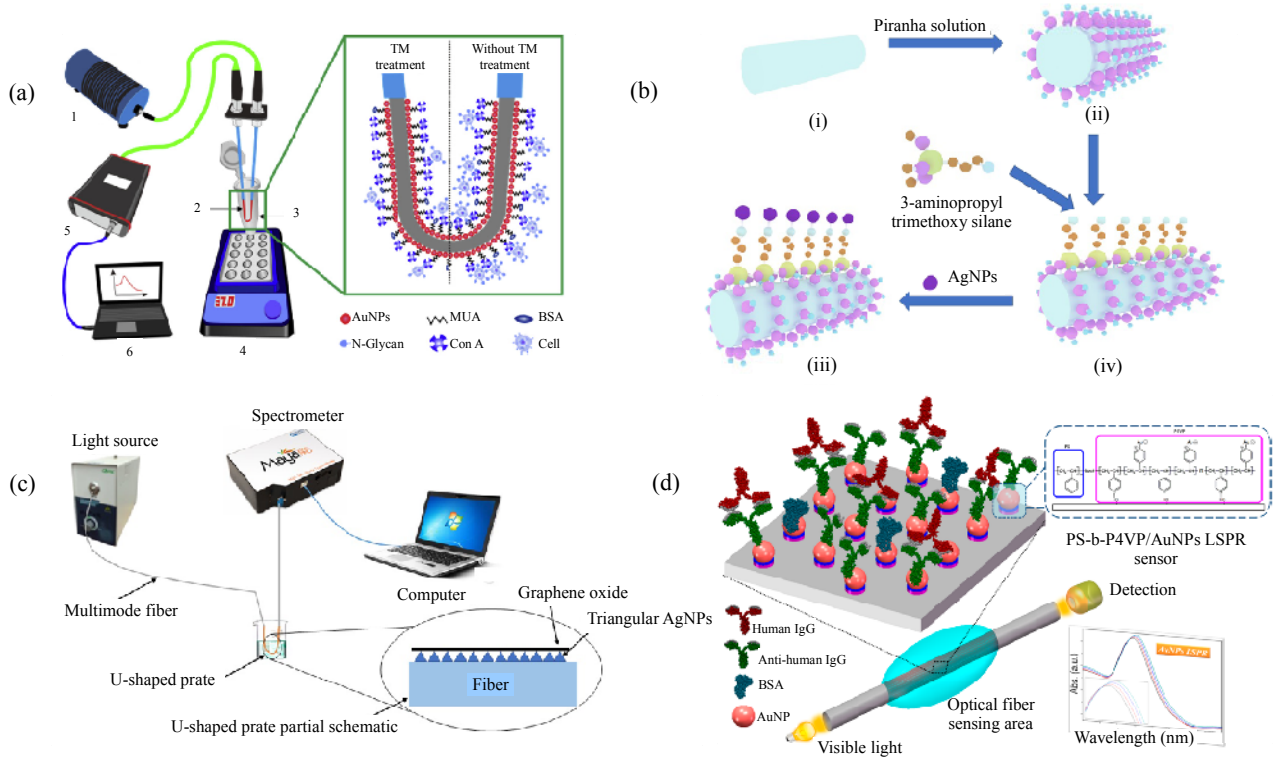

Fig. 11 LSPR part diagram: (a) U-shaped fiber LSPR system depicted in a schematic diagram (Fig. 1 in [78]), (b) schematic diagram of immobilizing silver nanoparticles on the fiber optic surface (Fig. 5 in [79]), (c) experimental system depicted in a schematic diagram (Fig. 7 in [79]), and (d) fiber optic LSPR sensor schematic diagram (Fig. 1 in [80]).

3.3 LRSPR sensors

On the basis of the SPR film layer structure, a specific electromagnetic field mode called the LRSPR is excited by inserting a matching dielectric layer between the substrate and the metal film, which has a narrower bandwidth and a higher detection accuracy than the SPR resonance spectrum.

In 2019, H. Zhang *et al*. [83] proposed an LRSPR sensor with the enhanced performance and applied it to biosensing. Compared to the CSPR sensor, the FOM of the LRSPR sensor is 1.14 times higher, according to the experimental data. The sensor is an LRSPR stimulated with a silver film and uses a laterally polished multimode fiber as a waveguide and MgF_2 as a buffer layer.

Self-compensation for temperature and an excellent quality factor D-type fiber optic LRSPR sensor using Q. Wang *et al.*'s [84] design was proposed in 2020. Figures 12(a)(i) and (a)(ii), respectively, show the detecting structures of the SPR sensor and the LRSPR sensor. In comparison to the SPR sensor, the results reveal an improvement in the sensitivity of 947.31 nm/RIU and a quality factor of 67.75 RIU^{-1}, which has promising applications in biochemistry. W. Luo *et al.* [85] created a D-type hexagonal structured PCF for an LRSPR sensor in 2021 based on a magnesium fluoride adsorbent layer (MgF_2). The results show that the LRSPR-based sensor has the greater sensitivity (–490.625% RIU^{-1}) along with the deeper penetration. A revolutionary hollow fiber temperature sensor (HFTS) based on the LRSPR was proposed by Y. X. Tang *et al.* [86] in the same year. The suggested system's structure is depicted in Fig. 12(b), where the HFTS is made up of two multimode fibers coupled at both ends and a hollow dielectric fiber with a silver coating that has been filled with a thermosensitive liquid. The experimental equipment for measuring the HFTS transmission spectra at various temperatures is depicted in Fig. 12(c). According to the results, the sensor is sensitive to changes in the temperature from 1.60 nm/℃ to 5.21 nm/℃ and has an FOM of up to 0.045 3 $℃^{-1}$ in the range of 20 ℃ to 60 ℃. The research's findings are extremely important for the study of fiber optic temperature sensors. Since the low sensitivity can limit the LRSPR sensor performance FOM, based on this, in 2022, Q. Wang *et al.* [87] introduced a low-dimensional nanostructure (Au nanosphere, WS_2) aided LRSPR sensor in an effort to boost the sensitivity and interfacial electric field of the LRSPR sensor. The RI sensing experiment of the WS_2-assisted LRSPR sensor is carried out. Figure 12(d) presents a schematic illustration of the manufacturing process for sensors. And the sensitivity is improved by 25.47% and the FOM is improved by 7.13%, while the gold nanosphere assisted LRSPR sensor shows an increase in the sensitivity by 29.23% and the FOM by 15.95%.

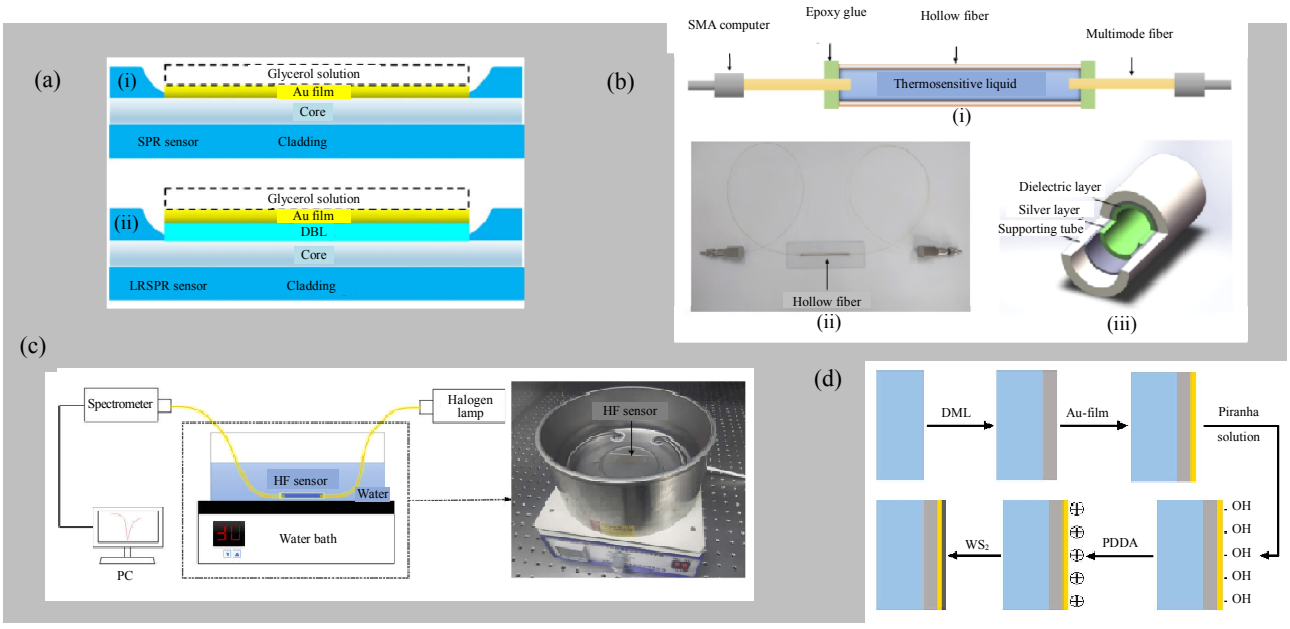

Fig. 12 LRSPR part diagram: (a): (i) SPR sensor and (ii) schematic representation of the LRSPR sensor's detecting structure (Fig. 10 in [84]); (b) structure of the presented HFTS system: (i) schematic, (ii) photograph, and (iii) HF's structural design (Fig. 1 in [86]); (c) experimental system in a schematic diagram (Fig. 3 in [86]); (d) process flow diagram for the production of sensors (Fig. 3 in [87]).

The LRSPR is an emerging technique that uses the physical effects of long-range plasmon exciton oscillations to achieve the detection of micron-scale samples. The LRSPR method has the advantages of high sensitivity, tunability, and resistance to light scattering, and can be used for the detection of non-homogeneous systems, which is a new method with a great potential for development. However, its implementation is relatively complicated in practical applications, and further research and development are needed in practical applications.

4. Application of fiber optic SPR biosensors

Owing to its high sensitivity, compact size, and ability to be configured for multiple channels and detect in real time, fiber optic SPR sensors have been extensively used in a number of industries involving health inspections, food safety inspections, environmental inspections, and marine fields.

4.1 Healthcare applications

Fiber optic SPR biosensors are employed in the health monitoring field [88] to find antigen antibodies [89, 90], miRNA [91], DNA hybridization [92, 93], glycoproteins [94], and other things.

In 2009, J. Pollet *et al*. [95] first combined fiber optic SPR sensors with DNA aptamer bioreceptors and showed that these fiber optic biosensors could be used not only for the quantification of DNA or proteins in biological samples, but also for real-time monitoring of binding and dissociation of biomolecular interactions. In 2017, N. F. Chiu *et al*. [96] demonstrated the carboxyl functionalized graphene oxide (GO-COOH) composites on the surface of sensing membranes to form a biocompatible potential for immunoaffinity SPR biosensors. Based on this, in 2018, Q. Wang *et al*. [97] used co-modified PCF, graphene oxide (GO), and staphylococcal protein A (SPA) to develop an enhanced SPR immunosensor enabling the detection of human IgG. The precise procedure for PCF surface amination and graphene oxide modification is depicted in Fig. 13(a), and additionally, the experimental results show that the LOD of human IgG can be as low as 10 ng/mL, and the graphene oxide modified PCF's RI sensitivity reaches 4649.8 nm/RIU, or about 1888 nm/RIU more sensitive than the RI sensitivity of the unmodified PCF. S. Qian *et al*. [98] employed PBA-AuNPs to selectively enhance the target miRNA signals in 2018 since it was challenging to detect miRNA directly on the sensing surface. Figure 13(b) shows an optical fiber SPR-based miRNA sensing system, and the outcomes demonstrate that the approach, with an LOD of 0.27 pM, has the great selectivity and sensitivity for miRNA. This PBA-AuNPs amplification mechanism can be used to detect RNA using a variety of sensing methods, including surface-enhanced Raman spectroscopy and electrochemistry. A staphylococcal protein A (SPA) and graphene oxide (GO)-based fiber-optic SPR biosensor with tilted fiber Bragg gratings (TFBG) co-modification was proposed by Q. Wang *et al*. [99] in 2019. The detection of human immunoglobulin G (IgG) using this sensor is the first time. For human IgG solutions with a concentration range of 30 g/mL to 100 g/mL and an LOD of 0.5 g/mL, the sensitivity of the proposed sensor is 0.096 dB/(g/mL), according to the experimental data shown in Fig. 13(c), and this also shows the TFBG-SPR biosensor modified by GO-SPA's sensing structure and manufacturing process. H. Song *et al*. [100] created a new optical fiber biosensor in 2020 employing MoS_2 nanosheets (fiber-MoS_2-gold film) positioned between the gold film and optical fiber in order to boost the sensitivity of SPR sensors and apply it to the detection of human IgG proteins. The findings show that the LOD may only be as low as 19.7 ng/mL, and Fig. 13(d) illustrates the construction of the biosensor used to detect IgG protein. In the following year, M. Chen *et al*. [101] introduced a D-type fiber optic biosensor that utilized the SPR for the detection of human immunoglobulin G (HIgG), and the results revealed that the sensor's sensitivity for the HIgG concentration was around 91 nm/(mg/ml).

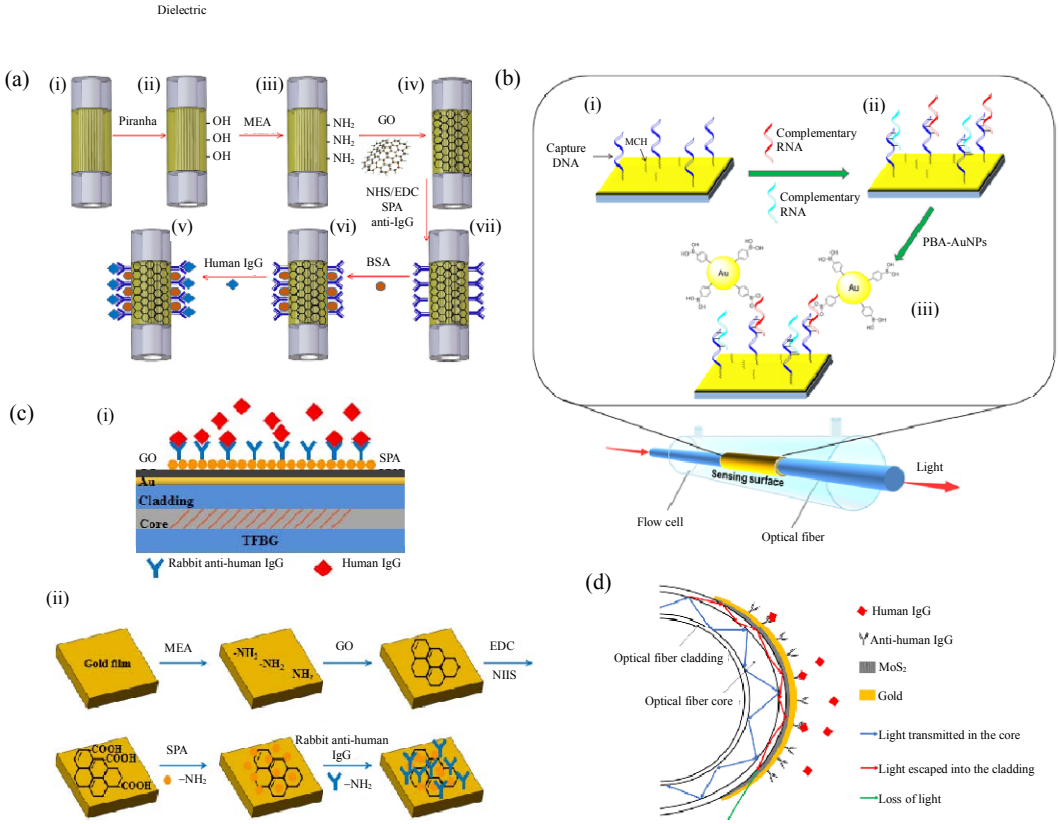

Fig. 13 Healthcare application section diagram: (a) IgG immunoassay method modified by graphene oxide and SPA (Fig. 2 in [97]); (b) schematic of a fiber-optic SPR sensor for detecting miRNAs: (i) the sensor surface's capture of DNA/MCH alteration, (ii) hybridization of DNA or RNA single-strands on the sensor surface, and (iii) selective binding of the RNA amplification signal by PBA-AuNPs (Fig. 1 in [98]); (c): (i) diagram of the sensing system and (ii) steps involved in creating a TFBG-SPR biosensor modified by GO-SPA (Fig. 6 in [99]); (d) schematic diagram of the IgG protein detection biosensor structure (Fig. 5 in [100]).

In 2023, for the first time, anti-human IgG was altered on the surface of a fiber optic SPR biosensor by S. Dai *et al.*'s [102] highly repeatable fiber optic SPR biosensor, which used carbon disulfide (CS_2) as a cross-linking agent. The sensing system is graphically depicted in Fig. 14(a), and the prepared multimode fiber-single mode fiber-reflector (MSR)-SPR biosensor's surface energy dispersive spectroscopy (EDS) and scanning electron microscope (SEM) diagrams are shown in Figs. 14(b) and 14(c), respectively. Figure 14(d) illustrates the biosensor's optimized final surface modification procedure.

4.2 Food applications

In food safety, fiber optic SPR biosensors are used to detect carcinogens [103, 104], allergens [105], enzymes [106], etc. in food products.

R. Slavik *et al.* [107] published a description of an SPR biosensor for staphylococcal enterotoxin B (SEB) detection in 2002. In less than 10 minutes, it has been shown to directly detect SEB concentrations of ng/ml. The first fiber optic SPR biosensor with the nanoparticle signal enhancement was described by J. Pollet *et al.* [108] in 2011 for the purpose of detecting the peanut allergen Ara h1. According to the findings, the biosensor LOD for Ara h1 increases by a further two orders of magnitude, rising from 9 g/mL for label-free detection to 0.21 g/mL for antibody sandwich detection to 0.09 g/mL to supply nanoparticle-enhanced detection. Monitoring illegal dyes in food requires sensitive detection methods, and in 2014, X. Y. Xu *et al.* [109] fabricated a molecularly imprinted polymer (MIP)

SPR sensor to detect Sudanese dyes. According to the results, Sudan dye could be detected by the MIPSPR sensor at an LOD of 30 ng mL^{-1} and at a sensitivity range of 50 ng mL^{-1}–400 ng mL^{-1}. S. Qian *et al*. [110] created the phenylboronic acid derivative (ABA-PBA) in 2015 to expand the scope of the fiber optic SPR sensing technology; afterward, they placed it on the modified SPR fiber optic sensor for carboxyl mercaptan to specifically detect glucose. Figure 15(a) shows the fiber optic sensor system's schematic architecture. The APA-BPA modified probe's LOD for the fructose solution is 0.2 mM during low concentrations (10 mM–50 mM). In the same year, R. Pilolli *et al*. [111] published a description of an SPR-based biosensor for the quick identification of egg-related abrasive allergens in wine, having a 0.03 g/mL–0.2 g/mL LOD.

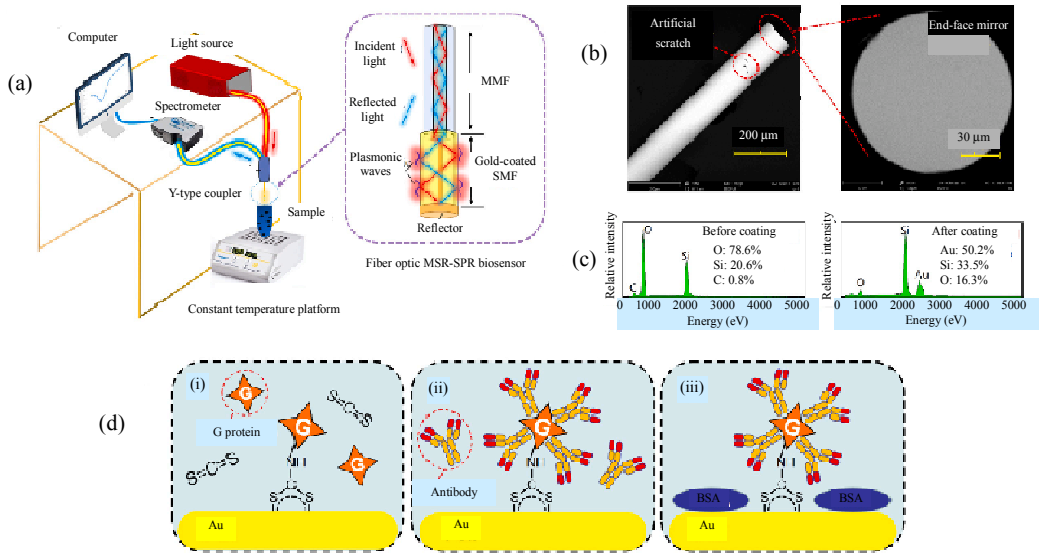

Fig. 14 Healthcare application section diagram: (a) sensing system's schematic diagram, (b) developed fiber optic MSR-SPR biosensor shown in an SEM image, (c) fiber optic MSR-SPR biosensor's sensing region contrasted using EDS before and after being coated with an Au layer, and (d) process of surface modification of the biosensor ([102], Fig. 1).

In order to identify milk allergies, J. Ashley *et al*. [112] developed an antibody-based α-casein SPR sensor in 2017. The sensor demonstrated the development and a potential of the α-casein-specific antibody SPR sensor with a good sensitivity at an LOD of 57.8 ng mL^{-1}. A very sensitive biosensor with selective D-sorbitol was developed by R. Kant *et al*. [113] who in the same year utilized Ta_2O_5 nanoflowers regarding fiber optic SPR and SDH enzyme-entrapped materials. The experimental system diagram is given in Fig. 15(b), producing, respectively, a sensitivity and an LOD of 92.16 nm/μg/mL and 3.6 ng/mL, and its performance demonstrates its potential for applications in the food industry. A nanosilver-reduced graphene oxide (AgNPs-rGO) and antimicrobial peptide (AMP) based optical fiber SPR resonance sensor was proposed by C. Zhou *et al*. [114] in 2018 for determining the presence of Escherichia coli O157:H7. The related figure is shown in Fig. 15(c), and it has a detection threshold of just 5×10^2 cfu/mL, making it a highly sensitive and quick method. In 2019, S. Kaushik *et al*. [115] reported the detection of E. coli via a molybdenum disulfide (MoS_2) nanosheet-functionalized fiber optic SPR immunosensor. The experimental system is depicted in Fig. 15(d), and the findings reveal that the detection platform is capable of sensitive detection of E. coli down to 94 CFU/mL.

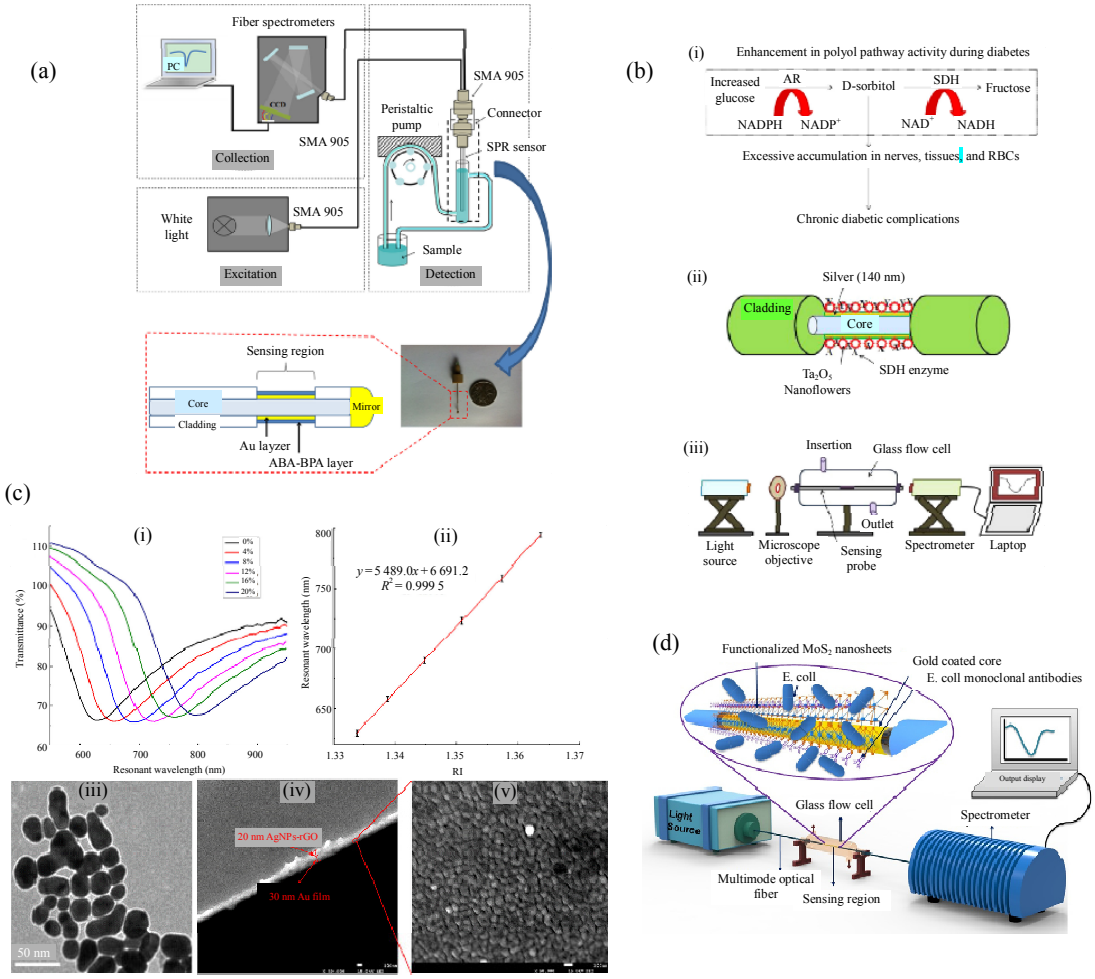

Fig. 15 Food application section diagram: (a) system schematic for the fiber optic SPR sensor (Fig. 1 in [110]); (b): (i) diagram of the polyol pathway that highlights the significance of D-sorbitol sensing, (ii) illustration of the fiber optic sensing probe in readiness, and (iii) illustration of the experimental setup in schematic form (Fig. 1 in [113]); (c): (i) sensor used to obtain the transmittance spectra of sucrose solutions with varied mass fractions using fiber optic SPR, (ii) maps of corrected resonance wavelength and RI for sucrose solutions using the fiber optic SPR sensor, (iii) AuNPs under transmission electron microscopy, and (iv) & (v) gold coatings on the surface of the fiber optic SPR sensor in scanning electron pictures (Fig. 2 in [114]); (d) experimental setup of the proposed fiber optic SPR immunosensor for the detection of E. coli is shown schematically (Fig. 1 in [115]).

4.3 Environment applications

For environmental monitoring, SPR biosensors with fiber optics are utilized to detect liquid concentrations, harmful gases, hazardous substance residues [116], heavy metal ions [117], agricultural environments [118], and the detection of ambient temperature and humidity [119] in the environment.

A special fiber optic SPR sensor with a sensitive coating made of palladium was proposed by C. Perrotton *et al.* [120] in 2011 for the purpose of detecting hydrogen in the environment. A schematic design of the suggested sensor with a resonance wavelength above 17.6 nm at the 4% hydrogen concentration for a multilayer material made of 35 nm silver, 100 nm silicon, and 3 nm palladium is shown in Fig. 16(a). According to Y. Zhao *et al.*'s [121] proposal in 2014 for an optical fiber SPR sensor for measuring liquid concentration, the experimental apparatus depicted in Fig. 16(b) was used to detect the volume concentration of a 0%–50% glycerol solution with a sensitivity range of 346.7 nm/%–890.7 nm/%. Using the association between SPR and water vapor condensation as a foundation, H. E. Limodehi *et al.* [122] created a multi-channel fiber optic dew moisture sensor in

2018, and Fig. 16(c)(i) is the transmitter image, while Fig. 16(c)(ii) is a cross-sectional view of the fiber optic probe. This sensor has the ability to identify the development of moisture or dew in real time through various places using its fiber optic channels, which is capable of accurately measuring the dew point temperature and relative humidity (RH) in multiple surroundings at once with a 5% margin of error. Monitoring of heavy metal ions in the solution in real time with the great sensitivity is crucial for environmental monitoring.

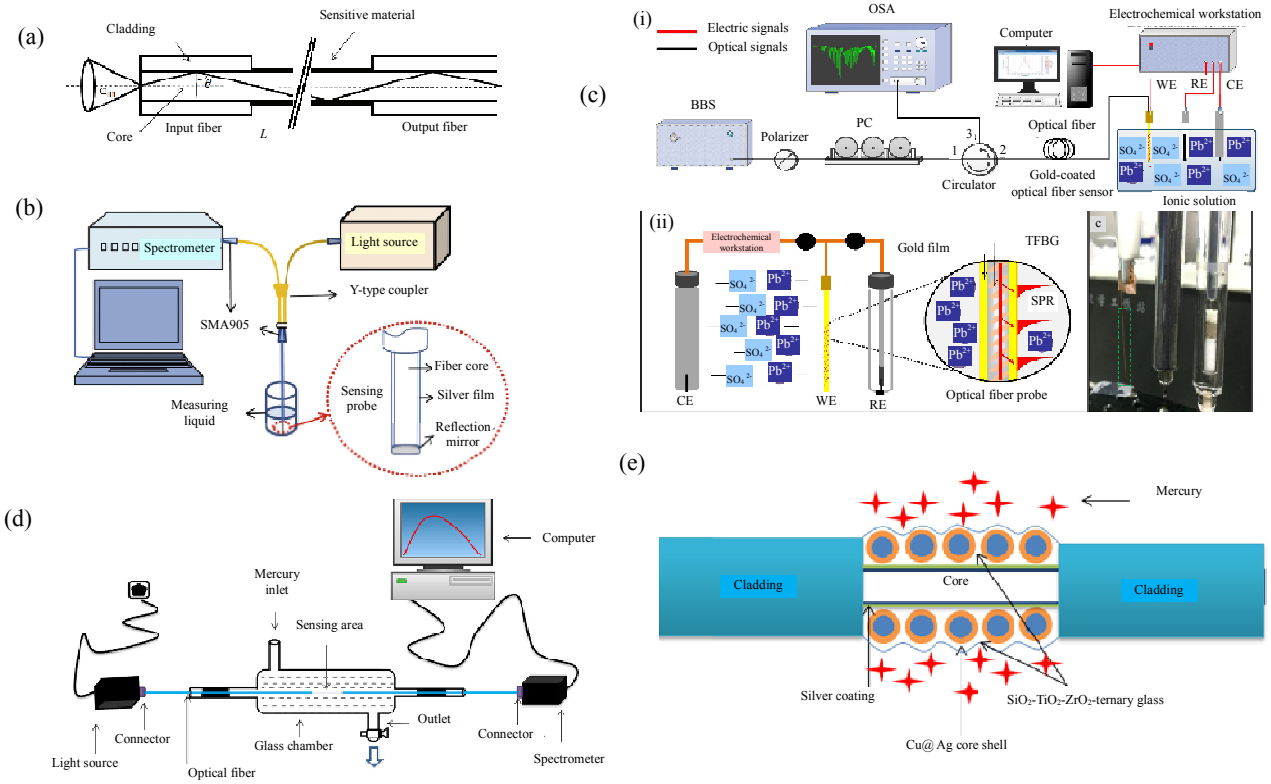

Fig. 16 Environment application section diagram: (a) diagrammatic representation of the delicate substance left on the fiber core after the cladding is removed (Fig. 1 in [120]); (b) experimental system illustrated in a schematic diagram (Fig. 2 in [121]); (c): (i) picture of the transmitter and (ii) cross-sectional view of the fiber probe (Fig. 2 in [108]); (d) fiber optic sensors used in an experimental mercury detection setup (Fig. 1 in [122]); (e) mercury detecting system shown schematically (Fig. 15 in [124]).

To address the noise and environmental interference problems of conventional electrochemical methods in detection, in 2019, Y. Si *et al*. [123] suggested a brand-new electrochemical SPR (EC-SPR) fiber optic sensor. For the intention of detecting mercury around copper and silver core-shell nanoparticles (Cu@Ag CNPs), V. P. Prakashan *et al*. [124] presented a certain SPR-based fiber optic sensor in 2020. Figure 16(d) displays a schematic representation of the entire sensor system. Cu@Ag CNPs are used as the sensing material to create the SPR-based fiber optic mercury sensor, and Fig. 16(e) depicts the sensing mechanism. It is discovered that the upper limit (10 nM) of the mercury level in water samples can be determined using the change in the transmittance intensity with increasing mercury content.

4.4 Ocean applications

In marine exploration, fiber optic SPR biosensors are used to detect parameters that include the environment in water [125], the temperature, salinity, and pressure of seawater [126].

In order to perform in situ salinity measurements in saltwater and show the viability of fiber optic SPR sensors for ocean monitoring, N. Diaz-Herrera *et al*. [127] created an optical apparatus in 2006, whose major component was a fiber optic sensor for the RI that was based on the SPR. Y. C. Kim *et al*.

[128] created an SPR sensor in 2011 that could be used to measure the salinity and dissolved organic carbon (DOC) in coastal waters, demonstrating that the proposed sensor is capable of collecting complementary data useful for distinguishing salinity and DOC in coastal waters. A deep-sea hydrothermal vent's environs could be monitored in situ and in real time using an optical fiber SPR sensor, as proposed by Y. C. Kim *et al*. [129] in 2012. The findings point to the potential for in situ SPR assessment for monitoring at hydrothermal vents and their surroundings, including the capacity to identify spatial gradients of dissolved hydrocarbons while vent fluid mixing. A new sensing technique for measuring the temperature and salinity of seawater simultaneously utilizing a C-type micro structure fiber was proposed by Y. Zhao *et al*. [130] in 2018, and the sensor's design was revealed. When the demodulator accuracy is 1 pm, the entire fabrication and filling process is depicted in Fig. 17(a), which easily reaches 10^{-6} and 10^{-3} resolutions in 5 ℃–35 ℃ and 30‰–40‰ saline ranges of saltwater, respectively. For the simultaneous measurement of temperature and saltwater salinity, E. Siyu *et al*. [131] suggested the development of a hollow fiber-based dual-channel surface SPR sensor in 2020. According to the experimental findings, the sensor has a temperature sensitivity of –0.956 nm/℃ in the range of values from 15 ℃ to 35 ℃ along with the salinity sensitivity of 0.3769 nm/‰ within the span of values of 0‰ to 40‰. In order to measure both the pressure and salinity, M. Yang *et al*. [132] suggested a fiber optic underwater sensor based on the SPR with multimode interference (MMI) in 2021. The SPR region in the fiber structure produces a resonant inclination for measuring salinity, while the separate MMI region produces a narrow and salinity-insensitive interferometric inclination to determine the pressure. According to the findings, the sensitivity to the pressure and salinity is –1.42 nm/MPa and 0.36 nm/‰, respectively.

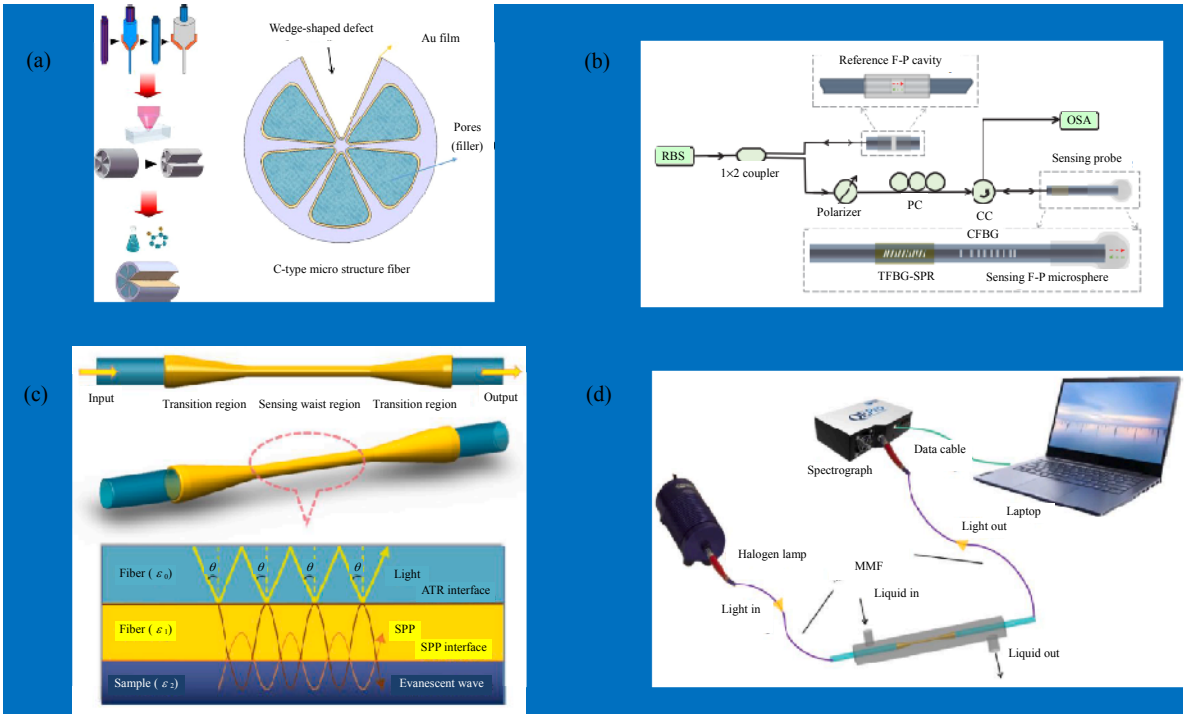

Fig. 17 Ocean application section diagram: (a) proposed sensor fabrication process (Fig. 2 in [130]), (b) proposed sensor scheme (Fig. 1 in [133]), (c) structure and sensing methodology of the tapered optical fiber-based SPR salinity sensor (Fig. 1in [134]), and (d) diagrammatic representation of the experimental apparatus for measuring salinity (Fig. 5 in [134]).

For the purpose of measuring the salinity, temperature, and depth (STD) of seawater simultaneously in 2023, G. An *et al*. [133] integrated a tilted fiber Bragg grating (TFBG), a chirped fiber Bragg grating (CFBG), and an SPR effect, as well as a vernier effect. The suggested sensor's schematic diagram is shown in Fig. 17(b). The experimental results show that the temperature sensitivity is 10.82 pm/℃, the salinity sensitivity is 0.122 nm/g/kg, the depth sensitivity is 116.85 pm/m, and the depth can be measured to 1 000 m or more. It is of great value to measure salinity in the ocean with the high accuracy. Therefore, X. Wei *et al*. [134] prepared a tapered optical fiber and applied it to maritime salinity detection. The SPR salinity sensor based on the tapered optical fiber is designed, and its sensing mechanism can be seen in Fig. 17(c), while Fig. 17(d) depicts the experimental setup. Its measurement sensitivity reaches 0.708 nm/‰ and has features of good linearity, reusability, and long-term use, and it provides the theoretical and technical basis for the development of the tapered fiber optic SPR salinity sensor.

5. Conclusions and outlook

This paper presents a comprehensive assessment of the fiber optic SPR biosensor research and applications. Firstly, the principles and excitation structures of SPR are introduced. Secondly, the existing fiber-optic SPR biosensors are classified, mainly from SPR, LSPR, and LRSPR, where SPR is introduced from both the structural sensitization and material sensitization. Finally, an overview of fiber-optic SPR biosensor applications is presented, which are analyzed from four aspects: health detection, food safety detection, environmental detection, and marine field. The experimental results for these applications show that fiber optic SPR sensors for biochemical sensing are of great value and can be developed for more detection substances.

Firstly, single-channel detection is the major application for fiber-optic SPR sensors, and multi-channel detection can be tried in the future to detect multiple parameters simultaneously more conveniently. SPR fiber optic biosensors can be combined with other technologies to achieve simultaneous detection of multiple parameters, improving the detection efficiency and accuracy. For example, scholars can combine the micro and nano technologies to build multiple micro and nano sensors with different functions and integrating them into a single optical fiber, thus realizing the simultaneous detection of multiple parameters. Secondly, it can detect in more fields and also detect more materials and parameters in the field of detection, so that it can play its role better and make greater contributions to human society. If it is applied to precision medicine, it can realize research on disease diagnosis, disease process monitoring, and efficacy evaluation, whose potential applications are in many fields. In the field of environmental monitoring, it can be applied to water quality monitoring, pollution monitoring, etc., to achieve real-time monitoring and analysis of environmental quality, thus contributing to the protection of the ecological environment. The SPR fiber optic sensing technology is a highly efficient method of drug screening and evaluation in the field of pharmaceutical development, which can be applied to the pathogenesis of diseases, the mechanism of action of drugs, and drug screening. On this basis, it can further enhance its sensitivity and broaden its detection range to achieve the higher sensitivity and higher detection accuracy. Consequently, fiber optic SPR sensors will be advanced and innovated in response to the creation of novel materials and technologies, and are expected to be utilized in a larger variety of fields and industries in the future.

Acknowledgment

This work was supported by the National Natural Science Foundation of China (Grant No. 62073068), the Fundamental Research Funds for the Central Universities (Grant No. N2204019), the

Applied Basic Research Program Project of Liaoning Province (Grant No. 2023JH2/101300179), the Research Fund of State Key Laboratory of Synthetical Automation for Process Industries (Grant No. 2018ZCX29), the Shenyang Science and Technology Plan Project (Grant No. 23-407-3-01), the Hebei Natural Science Foundation (Grant No. F2020501040), and the Natural Science Foundation of Shandong Province (Grant Nos. ZR2020MF108 and ZR2020MD058).

Declarations

Conflict of Interest The authors declare that they have no competing interests.

Permissions All the included figures, tables, or text passages that have already been published elsewhere have obtained the permission from the copyright owner(s) for both the print and online format.

References

[1] X. D. Wang and O. S. Wolfbeis, "Fiber-optic chemical sensors and biosensors (2008–2012)," *Analytical Chemistry*, 2013, 85(2): 487–508.

[2] X. Yang, C. Gong, C. Zhang, Y. Wang, G. F. Yan, L. Wei, *et al.*, "Fiber optofluidic microlasers: structures, characteristics, and applications," *Laser & Photonics Reviews*, 2022, 16(1): 2100171.

[3] C. Liang, J. Lai, S. Lou, H. Duan, and Y. Hu, "Resonant metasurfaces for spectroscopic detection: physics and biomedical applications," *Advanced Devices & Instrumentation*, 2022, 2022: 9874607.

[4] M. M. Moussilli, A. R. El Falou, R. M. Shubair, and Ieee, "On the design of graphene surface plasmon resonance sensors for medical applications," in *IEEE-Antennas-and-Propagation-Society Inter-National Symposium on Antennas and Propagation/USNC/URSI National Radio Science Meeting*, Boston, USA, 2018, pp. 1399–1400.

[5] V. Silin and A. Plant, "Biotechnological applications of surface plasmon resonance," *Trends in Biotechnology*, 1997, 15(9): 353–359.

[6] J. Homola, "Present and future of surface plasmon resonance biosensors," *Analytical and Bioanalytical Chemistry*, 2003, 377(3): 528–539.

[7] B. O. Liedberg, C. Nylander, I. J. S. Lundstrom, and Actuators, "Surface plasmon resonance for gas detection and biosensing," *Sensors and Actuators*, 1983, 4(83): 299–304.

[8] W. M. Mullett, E. P. Lai, and J. M. Yeung, "Surface plasmon resonance-based immunoassays," *Methods*, 2000, 22(1): 77–91.

[9] P. Mohankumar, J. Ajayan, T. Mohanraj, and R. Yasodharan, "Recent developments in biosensors for healthcare and biomedical applications: a review," *Measurement*, 2021, 167.

[10] B. Johnsson, S. Lofas, and G. Lindquist, "Immobilization of proteins to a carboxymethyldextran-modified gold surface for biospecific interaction analysis in surface plasmon resonance sensors," *Analytical Biochemistry*, 1991, 198(2): 268–277.

[11] A. Rezabakhsh, R. Rahbarghazi, and F. Fathi, "Surface plasmon resonance biosensors for detection of Alzheimer's biomarkers; an effective step in early and accurate diagnosis," *Biosensors & Bioelectronics*, 2020, 167: 112511.

[12] O. Esteban, A. Gonzalez-Cano, N. Diaz-Herrera, and M. C. Navarrete, "Absorption as a selective mechanism in surface plasmon resonance fiber optic sensors," *Optics Letters*, 2006, 31(21): 3089–3091.

[13] H. S. Jang, K. N. Park, C. D. Kang, J. P. Kim, S. J. Sim, and K. S. Lee, "Optical fiber SPR biosensor with sandwich assay for the detection of prostate specific antigen," *Optics Communications*, 2009, 282(14): 2827–2830.

[14] B. D. Gupta and R. K. Verma, "Surface plasmon resonance-based fiber optic sensors: principle, probe designs, and some applications," *Journal of Sensors*, 2009: 1–12.

[15] K. Kukanskis, J. Elkind, J. Melendez, T. Murphy, G. Miller, and H. Garner, "Detection of DNA hybridization using the TISPR-1 surface plasmon resonance biosensor," *Analytical Biochemistry*, 1999, 274(1): 7–17.

[16] M. Safdar, J. Spross, and J. Janis, "Microscale immobilized enzyme reactors in proteomics: latest developments," *Journal of Chromatography A*, 2014, 1324: 1–10.

[17] M. N. Mar, B. D. Ratner, and S. S. Yee, "An intrinsically protein-resistant surface plasmon resonance biosensor based upon a RF-plasma-deposited thin film," *Sensors and Actuators B: Chemical*, 1999, 54(1–2): 125–131.

[18] M. M. Morelock, R. H. Ingraham, R. Betageri, and S. Jakes, "Determination of receptor-ligand kinetic and equilibrium binding constants using surface plasmon resonance: application to the lck SH_2 domain and phosphotyrosyl peptides," *Journal of Medicinal*

Chemistry, 1995, 38(8): 1309–1318.
[19] R. Nuster, G. Paltauf, and P. Burgholzer, "Comparison of surface plasmon resonance devices for acoustic wave detection in liquid," *Optics Express*, 2007, 15(10): 6087–6095.
[20] X. Guo, "Surface plasmon resonance based biosensor technique: a review," *Journal of Biophotonics*, 2012, 5(7): 483–501.
[21] A. S. Barker, "Direct optical coupling to surface excitations," *Physical Review Letters*, 1972, 28(14): 892–895.
[22] R. A. Ferrell, "Predicted radiation of plasma oscillations in metal films," *Physical Review*, 1958, 111(5): 1214–1222.
[23] B. D. Gupta and R. K. Verma, "Surface plasmon resonance-based fiber optic sensors: principle, probe designs, and some applications," *Journal of Sensors*, 2009: 1–12.
[24] P. S. Pandey, Y. Singh, and S. K. Raghuwanshi, "Theoretical analysis of the LRSPR sensor with enhance FOM for low refractive index detection using MXene and fluorinated graphene," *IEEE Sensors Journal*, 2021, 21(21): 23979–23986.
[25] F. Mumtaz, B. Zhang, M. Roman, L. G. Abbas, M. A. Ashraf, and Y. Dai, "Computational study: windmill-shaped multi-channel SPR sensor for simultaneous detection of multi-analyte," *Measurement*, 2023, 207: 112386.
[26] J. Homola, I. Koudela, and S. S. Yee, "Surface plasmon resonance sensors based on diffraction gratings and prism couplers: sensitivity comparison," *Sensors and Actuators B: Chemical*, 1999, 54(1–2): 16–24.
[27] B. Hossain, A. Kumar Paul, M. Arefin Islam, M. Faruk Hossain, and M. Mahabubur Rahman, "Design and analysis of highly sensitive prism based surface plasmon resonance optical salinity sensor," *Results in Optics*, 2022, 7: 100217.
[28] E. Kretschmann, "The determination of the optical constants of metals by excitation of surface plasmons," *Zeitschrift für Physik A Hadrons and Nuclei*, 1971, 241(4): 313–324.
[29] S. Ekgasit, C. Thammacharoen, F. Yu, and W. Knoll, "Influence of the metal film thickness on the sensitivity of surface plasmon resonance biosensors," *Applied Spectroscopy*, 2016, 59: 661–667.
[30] E. K. Akowuah, T. Gorman, and S. Haxha, "Design and optimization of a novel surface plasmon resonance biosensor based on Otto configuration," *Optics Express*, 2009, 17(26): 23511–23521.
[31] H. S. Lee, T. Y. Seong, W. M. Kim, I. Kim, G. W. Hwang, W. S. Lee, *et al.*, "Enhanced resolution of a surface plasmon resonance sensor detecting C-reactive protein via a bimetallic waveguide-coupled mode approach," *Sensors and Actuators B: Chemical*, 2018, 266: 311–317.
[32] S. Long, E. Wang, M. Wu, H. Zhu, N. Xu, Y. Wang, *et al.*, "Sensing absorptive fluids with backside illuminated grating coupled SPR sensor fabricated by nanoimprint technology," *Sensors and Actuators A: Physical*, 2022, 337: 113416.
[33] E. Wijaya, C. Lenaerts, S. Maricot, J. Hastanin, S. Habraken, J. Vilcot, *et al.*, "Surface plasmon resonance-based biosensors: from the development of different SPR structures to novel surface functionalization strategies," *Current Opinion in Solid State and Materials Science*, 2011, 15(5): 208–224.
[34] R. C. Jorgenson and S. S. Yee, "A fiber-optic chemical sensor based on surface plasmon resonance," *Sensors and Actuators B: Chemical*, 1993, 12(3): 213–220.
[35] H. Esmaeilzadeh, E. Arzi, F. Légaré, M. Rivard, and A. Hassani, "A super continuum characterized high-precision SPR fiber optic sensor for refractometry," *Sensors and Actuators A: Physical*, 2015, 229: 8–14.
[36] R. Kashyap and G. Nemova, "Surface plasmon resonance-based fiber and planar waveguide sensors," *Journal of Sensors*, 2009: 1–9.
[37] N. M. Y. Zhang, K. Li, T. Zhang, P. Shum, Z. Wang, Z. Wang, *et al.*, "Electron-rich two-dimensional molybdenum trioxides for highly integrated plasmonic biosensing," *ACS Photonics*, 2017, 5(2): 347–352.
[38] D. Feng, W. Zhou, X. Qiao, and J. Albert, "High resolution fiber optic surface plasmon resonance sensors with single-sided gold coatings," *Optics Express*, 2016, 24(15): 16456.
[39] C. Liu, W. Su, Q. Liu, X. Lu, F. Wang, T. Sun, *et al.*, "Symmetrical dual D-shape photonic crystal fibers for surface plasmon resonance sensing," *Optics Express*, 2018, 26(7): 9039–9049.
[40] X. Chen, L. Xia, and C. Li, "Surface plasmon resonance sensor based on a novel D-shaped photonic crystal fiber for low refractive index detection," *IEEE Photonics Journal*, 2018, 10(1): 1–9.
[41] F. Mumtaz, M. Roman, B. Zhang, L. G. Abbas, Y. Dai, M. A. Ashraf, *et al.*, "MXene ($Ti_3C_2T_x$) coated highly-sensitive D-shaped photonic crystal fiber based SPR-biosensor," *Photonics and Nanostructures – Fundamentals and Applications*, 2022, 52: 101090.
[42] J. Gao, S. Jiang, W. Yang, R. Liu, J. Feng, Z. Zha, *et al.*, "Design a D-shaped single mode fiber SPR sensor with a composite nanostructure of HMM/monolayer graphene for DNA hybridization detection," *Optics & Laser Technology*, 2023, 158: 108854.
[43] B. D. Gupta, H. Dodeja, A. K. J. O. Tomar, and Q. Electronics, "Fibre-optic evanescent field absorption sensor based on a U-shaped probe," *Optical and*

Quantum Electronics, 1996, 28(11): 1629–1639.
[44] C. Zhang, Z. Li, S. Z. Jiang, C. H. Li, S. C. Xu, J. Yu, *et al*., "U-bent fiber optic SPR sensor based on graphene/AgNPs," *Sensors and Actuators B: Chemical*, 2017, 251: 127–133.
[45] Q. Wang, H. Song, A. Zhu, and F. Qiu, "A label-free and anti-interference dual-channel SPR fiber optic sensor with self-compensation for biomarker detection," *IEEE Transactions on Instrumentation and Measurement*, 2021, 70: 1–7.
[46] W. Zhang, M. Wu, X. Wang, Z. Tong, M. Dong, and G. Yan, "Temperature insensitive salinity sensor with U-shaped structure based on few-mode fiber," *Optical Fiber Technology*, 2023, 76.
[47] Z. H. Ren, Q. Wang, X. W. Cong, W. M. Zhao, J. R. Tang, L. Wang, *et al*., "A fiber SPR sensor with high comprehensive evaluation indicator based on core mismatched U-shaped and tapered arm," *Measurement*, 2023, 206: 112248.
[48] R. A. Kadhim, A. K. K. Abdul, and L. Yuan, "Advances in surface plasmon resonance-based plastic optical fiber sensors," *IETE Technical Review*, 2020, 39: 442–459.
[49] Y. Zhao, L. Cai, and H. F. Hu, "Fiber-optic refractive index sensor based on multi-tapered SMS fiber structure," *IEEE Sensors Journal*, 2015, 15(11): 6348–6353.
[50] Y. Al-Qazwini, A. S. M. Noor, M. H. Yaacob, S. W. Harun, and M. A. Mahdi, "Experimental realization and performance evaluation of refractive index SPR sensor based on unmasked short tapered multimode-fiber operating in aqueous environments," *Sensors and Actuators A: Physical*, 2015, 236: 38–43.
[51] N. Goswami, K. K. Chauhan, and A. Saha, "Analysis of surface plasmon resonance based bimetal coated tapered fiber optic sensor with enhanced sensitivity through radially polarized light," *Optics Communications*, 2016, 379: 6–12.
[52] C. Teng, M. Li, R. Min, S. Deng, M. Chen, M. Xue, *et al*., "A high-sensitivity SPR sensor based on MMF-tapered HCF-MMF fiber structure for refractive index sensing," *IEEE Sensors Journal*, 2022, 22(19): 18517–18523.
[53] Z. Yang, L. Xia, C. Li, X. Chen, and D. Liu, "A surface plasmon resonance sensor based on concave-shaped photonic crystal fiber for low refractive index detection," *Optics Communications*, 2019, 430: 195–203.
[54] L. Li, Y. Wei, X. Zhao, C. Liu, R. Wang, T. Jiang, *et al.*, "Dual-channel step multimode fiber SPR sensor based on sawtooth structure," *Optical Fiber Technology*, 2022, 71: 102897.
[55] N. Cennamo, F. Arcadio, M. Seggio, D. Maniglio, L. Zeni, and A. M. Bossi, "Spoon-shaped polymer waveguides to excite multiple plasmonic phenomena: a multisensor based on antibody and molecularly imprinted nanoparticles to detect albumin concentrations over eight orders of magnitude," *Biosensors & Bioelectronics*, 2022, 217: 114707.
[56] L. Li, Y. Wei, W. Tan, Y. Zhang, C. Liu, Z. Ran, *et al*., "Fiber cladding SPR sensor based on V-groove structure," *Optics Communications*, 2023, 526: 128944.
[57] S. Zhang, Y. Peng, X. Wei, and Y. Zhao, "High-sensitivity biconical optical fiber SPR salinity sensor with a compact size by fiber grinding technique," *Measurement*, 2022, 204: 112156.
[58] Y. Wei, X. Zhao, C. Liu, R. Wang, T. Jiang, L. Li, *et al.*, "Fiber cladding dual channel surface plasmon resonance sensor based on S-type fiber," *Chinese Physics B*, 2023, 32(3): 030702.
[59] X. Jiang and Q. Wang, "Refractive index sensitivity enhancement of optical fiber SPR sensor utilizing layer of MWCNT/PtNPs composite," *Optical Fiber Technology*, 2019, 51: 118–124.
[60] C. Liu, Y. Gao, Y. Gao, Y. Wei, P. Wu, and Y. Su, "Enhanced sensitivity of fiber SPR sensor by metal nanoparticle," *Sensor Review*, 2020, 40(3): 355–361.
[61] Q. Wang, X. W. Cong, W. M. Zhao, Z. H. Ren, N. N. Du, X. Yan, *et al*., "High figure of merit SPR sensor based on raspberry-like silica," *IEEE Transactions on Instrumentation and Measurement*, 2022, 71: 1–8.
[62] A. K. Mishra, S. K. Mishra, and R. K. Verma, "Doped single-wall carbon nanotubes in propagating surface plasmon resonance-based fiber optic refractive index sensing," *Plasmonics*, 2016, 12(6): 1657–1663.
[63] J. Y. Jing, Q. Wang, and B. T. Wang, "Refractive index sensing characteristics of carbon nanotube-deposited photonic crystal fiber SPR sensor," *Optical Fiber Technology*, 2018, 43: 137–144.
[64] M. Luo and Q. Wang, "A reflective optical fiber SPR sensor with surface modified hemoglobin for dissolved oxygen detection," *Alexandria Engineering Journal*, 2021, 60(4): 4115–4120.
[65] M. F. Naief, Y. H. Khalaf, and A. M. Mohammed, "Novel photothermal therapy using multi-walled carbon nanotubes and platinum nanocomposite for human prostate cancer PC_3 cell line," *Journal of Organometallic Chemistry*, 2022, 975: 122422.
[66] Q. Wang, A. Zhu, F. Qiu, L. Wang, X. Y. Yin, W. M. Zhao, *et al*., "High sensitivity coreless fiber surface plasmon resonance sensor based on Au Nano biconical particles," *IEEE Sensors Journal*, 2022, 22(1): 256–263.
[67] H. Fu, S. Zhang, H. Chen, and J. Weng, "Graphene enhances the sensitivity of fiber-optic surface plasmon resonance biosensor," *IEEE Sensors Journal*, 2015, 15(10): 5478–5482.
[68] Q. Wang and B. T. Wang, "Surface plasmon resonance biosensor based on graphene oxide/silver

coated polymer cladding silica fiber," *Sensors and Actuators B: Chemical*, 2018, 275: 332–338.

[69] M. S. Rahman, S. S. Noor, M. S. Anower, L. F. Abdulrazak, M. M. Rahman, and K. A. Rikta, "Design and numerical analysis of a graphene-coated fiber-optic SPR biosensor using tungsten disulfide," *Photonics and Nanostructures – Fundamentals and Applications*, 2019, 33: 29–35.

[70] Q. Wang, X. Jiang, L. Y. Niu, and X. C. Fan, "Enhanced sensitivity of bimetallic optical fiber SPR sensor based on MoS_2 nanosheets," *Optics and Lasers in Engineering*, 2020, 128: 105997.

[71] T. Li, L. Zhu, L. Lu, R. You, X. Bian, G. Ren, *et al*., "Highly sensitive optical fiber plasmonic sensors by integrating hydrogen doped molybdenum oxide," *IEEE Sensors Journal*, 2022, 22(8): 7734–7742.

[72] H. H. Jeong, Y. J. Son, S. K. Kang, H. J. Kim, H. J. Roh, N. Erdene, *et al*., "Fiber-optic refractive index sensor based on the cone-based round structure," *IEEE Sensors Journal*, 2013, 13(1): 351–358.

[73] M. Rani, N. K. Sharma, and V. Sajal, "Localized surface plasmon resonance based fiber optic sensor with nanoparticles," *Optics Communications*, 2013, 292: 92–100.

[74] M. H. Tu, T. Sun, and K. T. V. Grattan, "LSPR optical fibre sensors based on hollow gold nanostructures," *Sensors and Actuators B: Chemical*, 2014, 191: 37–44.

[75] Y. J. He, "Novel and high-performance LSPR biochemical fiber sensor," *Sensors and Actuators B: Chemical*, 2015, 206: 212–219.

[76] S. Jiang, Z. Li, C. Zhang, S. Gao, Z. Li, H. Qiu, *et al*., "A novel U-bent plastic optical fibre local surface plasmon resonance sensor based on a graphene and silver nanoparticle hybrid structure," *Journal of Physics D: Applied Physics*, 2017, 50(16): 165105.

[77] H. M. Kim, M. Uh, D. H. Jeong, H. Y. Lee, J. H. Park, and S. K. Lee, "Localized surface plasmon resonance biosensor using nanopatterned gold particles on the surface of an optical fiber," *Sensors and Actuators B: Chemical*, 2019, 280: 183–191.

[78] Z. Luo, Y. Wang, Y. Xu, X. Wang, Z. Huang, J. Chen, *et al*., "Ultrasensitive U-shaped fiber optic LSPR cytosensing for label-free and in situ evaluation of cell surface N-glycan expression," *Sensors and Actuators B: Chemical*, 2019, 284: 582–588.

[79] H. Song, H. Zhang, Z. Sun, Z. Ren, X. Yang, and Q. Wang, "Triangular silver nanoparticle U-bent fiber sensor based on localized surface plasmon resonance," *AIP Advances*, 2019, 9(8): 085307.

[80] M. Lu, H. Zhu, C. G. Bazuin, W. Peng, and J. F. Masson, "Polymer-templated gold nanoparticles on optical fibers for enhanced-sensitivity localized surface plasmon resonance biosensors," *ACS Sensors*, 2019, 4(3): 613–622.

[81] H. M. Kim, J. H. Park, and S. K. Lee, "Fabrication and measurement of fiber optic localized surface plasmon resonance sensor based on hybrid structure of dielectric thin film and bilayered gold nanoparticles," *IEEE Transactions on Instrumentation and Measurement*, 2021, 70: 1–8.

[82] G. Li, Q. Xu, R. Singh, W. Zhang, C. Marques, Y. Xie, *et al*., "Graphene oxide/multiwalled carbon nanotubes assisted serial quadruple tapered structure-based LSPR sensor for glucose detection," *IEEE Sensors Journal*, 2022, 22(17): 16904–16911.

[83] H. Zhang, Y. Chen, X. Feng, X. Xiong, S. Hu, Z. Jiang, *et al*., "Long-range surface plasmon resonance sensor based on side-polished fiber for biosensing applications," *IEEE Journal of Selected Topics in Quantum Electronics*, 2019, 25(2): 1–9.

[84] Q. Wang, J. Y. Jing, X. Z. Wang, L. Y. Niu, and W. M. Zhao, "A D-shaped fiber long-range surface plasmon resonance sensor with high *Q*-factor and temperature self-compensation," *IEEE Transactions on Instrumentation and Measurement*, 2020, 69(5): 2218–2224.

[85] W. Luo, J. Meng, X. Li, D. Yi, F. Teng, Y. Wang, *et al*., "Long-range surface plasmon resonance sensor based on side-polished D-shaped hexagonal structure photonic crystal fiber with the buffer layer of magnesium fluoride," *Journal of Physics D: Applied Physics*, 2021, 54(50): 505106.

[86] Y. X. Tang, X. Zhang, X. S. Zhu, and Y. W. Shi, "Dielectric layer thickness insensitive EVA/Ag-coated hollow fiber temperature sensor based on long-range surface plasmon resonance," *Optics Express*, 2021, 29(1): 368–376.

[87] Q. Wang, X. W. Cong, Z. Cheng, W. M. Zhao, L. Wang, X. Y. Yin, *et al*., "Low dimensional nanostructure-assisted long-range surface plasmon resonance sensors with high figure of merit," *IEEE Transactions on NanoBioscience*, 2023, 22(1): 45–51.

[88] Z. Dai, J. Tan, K. Zhou, L. Zhang, X. Zhou, and Y. Tan, "Optical fiber SPR biosensor with frequency multiplexing compensated laser heterodyne feedback for ultrasensitive detection of fluoroquinolones," *Sensors and Actuators B: Chemical*, 2023, 393: 134335.

[89] A. Sadana and A. Ramakrishnan, "A kinetic study of analyte-receptor binding and dissociation for biosensor applications: a fractal analysis for cholera toxin and peptide-protein interactions," *Sensors and Actuators B: Chemical*, 2002, 85(1–2): 61–72.

[90] Y. Wang, C. Gong, X. Yang, T. Zhu, K. Zhang, Y. J. Rao, *et al.*, "Photonic bandgap fiber microlaser with dual-band emission for integrated optical tagging and sensing," *Laser & Photonics Reviews*, 2023, 17: 2200834.

[91] A. Azzouz, L. Hejji, K. H. Kim, D. Kukkar, B. Souhail, N. Bhardwaj, *et al*., "Advances in surface plasmon resonance-based biosensor technologies for

cancer biomarker detection," *Biosensors & Bioelectronics*, 2022, 197: 113767.

[92] K. N. Shushama, M. M. Rana, R. Inum, and M. B. Hossain, "Graphene coated fiber optic surface plasmon resonance biosensor for the DNA hybridization detection: Simulation analysis," *Optics Communications*, 2017, 383: 186–190.

[93] H. Torun, B. Bilgin, M. Ilgu, N. Batur, M. Ozturk, T. Barlas, *et al.*, "Rapid nanoplasmonic-enhanced detection of SARS-CoV-2 and variants on DNA aptamer metasurfaces," *Advanced Devices & Instrumentation*, 2023, 4: 0008.

[94] R. Wang, C. Liu, Y. Wei, Z. Ran, T. Jiang, C. Liu, *et al.*, "Fiber SPR biosensor sensitized by MOFs for MUC1 protein detection," *Talanta*, 2023, 258: 124467.

[95] J. Pollet, F. Delport, K. P. F. Janssen, K. Jans, G. Maes, H. Pfeiffer, *et al*., "Fiber optic SPR biosensing of DNA hybridization and DNA-protein interactions," *Biosensors & Bioelectronics*, 2009, 25(4): 864–869.

[96] N. F. Chiu, S. Y. Fan, C. D. Yang, and T. Y. Huang, "Carboxyl-functionalized graphene oxide composites as SPR biosensors with enhanced sensitivity for immunoaffinity detection," *Biosensors & Bioelectronics*, 2017, 89(Pt 1): 370–376.

[97] Q. Wang and B. Wang, "Sensitivity enhanced SPR immunosensor based on graphene oxide and SPA co-modified photonic crystal fiber," *Optics & Laser Technology*, 2018, 107: 210–215.

[98] S. Qian, M. Lin, W. Ji, H. Yuan, Y. Zhang, Z. Jing, *et al*., "Boronic acid functionalized Au nanoparticles for selective microRNA signal amplification in fiber-optic surface plasmon resonance sensing system," *ACS Sensors*, 2018, 3(5): 929–935.

[99] Q. Wang, J. Y. Jing, and B. T. Wang, "Highly sensitive SPR biosensor based on graphene oxide and staphylococcal protein a co-modified TFBG for human IgG detection," *IEEE Transactions on Instrumentation and Measurement*, 2019, 68(9): 3350–3357.

[100] H. Song, Q. Wang, and W. M. Zhao, "A novel SPR sensor sensitivity-enhancing method for immunoassay by inserting MoS_2 nanosheets between metal film and fiber," *Optics and Lasers in Engineering*, 2020, 132: 106135.

[101] M. Chen, T. Lang, B. Cao, Y. Yu, and C. Shen, "D-type optical fiber immunoglobulin G sensor based on surface plasmon resonance," *Optics & Laser Technology*, 2020, 131: 106445.

[102] S. Dai, X. Li, Y. Chen, J. Zhang, and X. Hong, "Highly reproducible fiber optic surface plasmon resonance biosensors modified by CS_2 for disposable immunoassays," *Sensors and Actuators B: Chemical*, 2023, 374: 132801.

[103] W. Yang, Y. Cheng, M. Jiang, S. Jiang, R. Liu, J. Lu, *et al*., "Design and fabrication of an ultra-sensitive Ta_2C MXene/Au-coated tilted grating sensor," *Sensors and Actuators B: Chemical*, 2022, 369: 132391.

[104] N. Masdor, Z. Altintas, and I. Tothill, "Surface plasmon resonance immunosensor for the detection of campylobacter jejuni," *Chemosensors*, 2017, 5(2): 16–30.

[105] J. Zhou, Q. Qi, C. Wang, Y. Qian, G. Liu, Y. Wang, *et al*., "Surface plasmon resonance (SPR) biosensors for food allergen detection in food matrices," *Biosensors & Bioelectronics*, 2019, 142: 111449.

[106] J. Zhang, X. Mai, X. Hong, Y. Chen, and X. Li, "Optical fiber SPR biosensor with a solid-phase enzymatic reaction device for glucose detection," *Sensors and Actuators B: Chemical*, 2022, 366: 131984.

[107] R. Slavik, J. Homola, and E. Brynda, "A miniature fiber optic surface plasmon resonance sensor for fast detection of staphylococcal enterotoxin B," *Biosensors & Bioelectronics*, 2002, 17(6–7): 591–595.

[108] J. Pollet, F. Delport, K. P. F. Janssen, D. T. Tran, J. Wouters, T. Verbiest, *et al*., "Fast and accurate peanut allergen detection with nanobead enhanced optical fiber SPR biosensor," *Talanta*, 2011, 83(5): 1436–1441.

[109] X. Y. Xu, X. G. Tian, L. G. Cai, Z. L. Xu, H. T. Lei, H. Wang, *et al*., "Molecularly imprinted polymer based surface plasmon resonance sensors for detection of Sudan dyes," *Analytical Methods*, 2014, 6(11): 3751–3757.

[110] S. Qian, Y. Liang, J. Ma, Y. Zhang, J. Zhao, and W. Peng, "Boronic acid modified fiber optic SPR sensor and its application in saccharide detection," *Sensors and Actuators B: Chemical*, 2015, 220: 1217–1223.

[111] R. Pilolli, A. Visconti, and L. Monaci, "Rapid and label-free detection of egg allergen traces in wines by surface plasmon resonance biosensor," *Analytical and Bioanalytical Chemistry*, 2015, 407(13): 3787–3797.

[112] J. Ashley, M. Piekarska, C. Segers, L. Trinh, T. Rodgers, R. Willey, *et al*., "An SPR based sensor for allergens detection," *Biosensors & Bioelectronics*, 2017, 88: 109–113.

[113] R. Kant, R. Tabassum, and B. D. Gupta, "A highly sensitive and distinctly selective D-sorbitol biosensor using SDH enzyme entrapped Ta_2O_5 nanoflowers assembly coupled with fiber optic SPR," *Sensors and Actuators B: Chemical*, 2017, 242: 810–817.

[114] C. Zhou, H. Zou, M. Li, C. Sun, D. Ren, and Y. Li, "Fiber optic surface plasmon resonance sensor for detection of E. coli O157:H7 based on antimicrobial peptides and AgNPs-rGO," *Biosensors & Bioelectronics*, 2018, 117: 347–353.

[115] S. Kaushik, U. K. Tiwari, S. S. Pal, and R. K. Sinha, "Rapid detection of Escherichia coli using fiber optic surface plasmon resonance immunosensor based on biofunctionalized molybdenum disulfide (MoS_2) nanosheets," *Biosensors & Bioelectronics*, 2019, 126: 501–509.

[116] Y. Guo, R. Liu, Y. Liu, D. Xiang, Y. Liu, W. Gui, *et al*., "A non-competitive surface plasmon resonance immunosensor for rapid detection of triazophos residue in environmental and agricultural samples," *Science of the Total Environment*, 2018, 613: 783–791.

[117] H. Yuan, W. Ji, S. Chu, Q. Liu, S. Qian, J. Guang, *et al*., "Mercaptopyridine-functionalized gold nanoparticles for fiber-optic surface plasmon resonance Hg^{2+} sensing," *ACS Sensors*, 2019, 4(3): 704–710.

[118] L. S. Goh, N. Kumekawa, K. Watanabe, and N. Shinomiya, "Hetero-core spliced optical fiber SPR sensor system for soil gravity water monitoring in agricultural environments," *Computers and Electronics in Agriculture*, 2014, 101: 110–117.

[119] Y. Wang, J. Li, L. N. Guo, M. Tian, and F. Meng, "Development of fabrication technique and sensing performance of optical fiber humidity sensors in the most recent decade," *Measurement*, 2023, 215: 112888.

[120] C. Perrotton, N. Javahiraly, M. Slaman, B. Dam, and P. Meyrueis, "Fiber optic surface plasmon resonance sensor based on wavelength modulation for hydrogen sensing," *Optics Express*, 2011, 19(23): A1175–A1183.

[121] Y. Zhao, Z. Q. Deng, and Q. Wang, "Fiber optic SPR sensor for liquid concentration measurement," *Sensors and Actuators B: Chemical*, 2014, 192: 229–233.

[122] H. E. Limodehi, M. Mozafari, H. Amiri, and F. Légaré, "Multi-channel fiber optic dew and humidity sensor," *Optical Fiber Technology*, 2018, 41: 89–94.

[123] Y. Si, J. Lao, X. Zhang, Y. Liu, S. Cai, Á. González-Vila, *et al*., "Electrochemical plasmonic fiber-optic sensors for ultra-sensitive heavy metal detection," *Journal of Lightwave Technology*, 2019, 37(14): 3495–3502.

[124] V. P. Prakashan, G. George, M. S. Sanu, M. S. Sajna, A. C. Saritha, C. Sudarsanakumar, *et al*., "Investigations on SPR induced Cu@Ag core shell doped SiO_2-TiO_2-ZrO_2 fiber optic sensor for mercury detection," *Applied Surface Science*, 2020, 507: 144957.

[125] C. Boulart, R. Prien, V. Chavagnac, and J. P. Dutasta, "Sensing dissolved methane in aquatic environments: an experiment in the central Baltic Sea using surface plasmon resonance," *Environmental Science & Technology*, 2013, 47(15): 8582–8590.

[126] C. R. Uma Kumari, D. Samiappan, R. Kumar, and T. Sudhakar, "Development of a highly accurate and fast responsive salinity sensor based on Nuttall apodized fiber Bragg grating coated with hygroscopic polymer for ocean observation," *Optical Fiber Technology*, 2019, 53: 102036.

[127] N. Díaz-Herrera, O. Esteban, M. C. Navarrete, M. L. Haitre, and A. González-Cano, "In situ salinity measurements in seawater with a fibre-optic probe," *Measurement Science and Technology*, 2006, 17(8): 2227–2232.

[128] Y. C. Kim, J. A. Cramer, and K. S. Booksh, "Investigation of a fiber optic surface plasmon spectroscopy in conjunction with conductivity as an in situ method for simultaneously monitoring changes in dissolved organic carbon and salinity in coastal waters," *Analyst*, 2011, 136(20): 4350–4356.

[129] Y. C. Kim, J. Cramer, T. Battaglia, J. A. Jordan, S. N. Banerji, W. Peng, *et al*., "Investigation of in situ surface plasmon resonance spectroscopy for environmental monitoring in and around deep-sea hydrothermal vents," *Analytical Letters*, 2013, 46(10): 1607–1617.

[130] Y. Zhao, Q. L. Wu, and Y. N. Zhang, "Theoretical analysis of high-sensitive seawater temperature and salinity measurement based on C-type micro-structured fiber," *Sensors and Actuators B: Chemical*, 2018, 258: 822–828.

[131] E. Siyu, Y. N. Zhang, B. Han, W. Zheng, Q. L. Wu, and H. K. Zheng, "Two-channel surface plasmon resonance sensor for simultaneous measurement of seawater salinity and temperature," *IEEE Transactions on Instrumentation and Measurement*, 2020, 69(9): 7191–7199.

[132] M. Yang, Y. Zhu, and R. An, "Underwater fiber-optic salinity and pressure sensor based on surface plasmon resonance and multimode interference," *Applied Optics*, 2021, 60(30): 9352–9357.

[133] G. An, L. Liu, P. Hu, P. Jia, F. Zhu, Y. Zhang, *et al*., "Probe type TFBG-excited SPR fiber sensor for simultaneous measurement of multiple ocean parameters assisted by CFBG," *Optics Express*, 2023, 31(3): 4229–4237.

[134] X. Wei, Y. Peng, X. Chen, S. Zhang, and Y. Zhao, "Optimization of tapered optical fiber sensor based on SPR for high sensitivity salinity measurement," *Optical Fiber Technology*, 2023, 78: 103309.